EUROPEAN JOURNAL OF PURE AND APPLIED MATHEMATICS
2025, Vol. 18, Issue 4, Article Number 7095
ISSN 1307-5543 – ejpam.com
Published by New York Business Global

A Laplace-Chebyshev Spectral Method for Multi-Dimensional Anomalous Transport

Kamran[1,*], Bibi Zahra[1], Zeeshan Ali[2], Ahmad Aloqaily[3], Nabil Mlaiki[3]

[1] *Department of Mathematics, Islamia College Peshawar, Peshawar 25120, Khyber Pakhtunkhwa, Pakistan*
[2] *Department of Information Management, National Yunlin University of Science and Technology, Douliu, Taiwan, Republic of China*
[3] *Department of Mathematics and Sciences, Prince Sultan University, P.O. Box 66833, Riyadh 11586, Saudi Arabia*

Abstract. Anomalous transport processes, such as subsurface contaminant spread or wave attenuation in viscoelastic materials, are governed by time-fractional diffusion-wave equations. The non-local nature of fractional operators and the high computational cost of addressing multi-dimensional spaces pose significant challenges for numerical simulations. To overcome this, we develop a novel hybrid spectral method combining the Laplace transform (LT) technique with the Chebyshev spectral collocation method (CSCM) for solving TFDWEs featuring the modified Atangana-Baleanu-Caputo derivative, chosen for its non-singular kernel and efficiency in modeling complex memory effects. Our numerical scheme, temporal and spatial discretizations, are decoupled. The LT handles the fractional time derivative exactly in the Laplace domain, removing time-stepping restrictions and convolution costs, while the CSCM ensures the exponential convergence in the spatial domain. The numerical inversion of LT is obtained using the improved Talbot method, guaranteeing rapid $O(e^{-c\mathrm{N}})$ convergence. This work provides not only a robust computational technique but also a rigorous mathematical analysis, establishing clear conditions for the existence, uniqueness, and Ulam-Hyers stability of the solutions. The dimensional flexibility of our technique is demonstrated through 1D, 2D, and 3D numerical examples, which confirm its computational efficiency and high accuracy. This work provides a robust and stable numerical approach that can be extended to model complex multi-scale transport problems across applied mathematics and engineering.

2020 Mathematics Subject Classifications: 44A10, 65R10, 35A22

Key Words and Phrases: Diffusion-wave equation, modified Atangana-Baleanu derivative, Laplace transform, Chebyshev spectral method, Talbot's method, uniqueness and existence

*Corresponding author.
DOI: https://doi.org/10.29020/nybg.ejpam.v18i4.7095

Email addresses: kamran.maths@icp.edu.pk (Kamran),
zeeshan@yuntech.edu.tw (Z. Ali),
maloqaily@psu.edu.sa (A. Aloqaily),
nmlaiki@psu.edu.sa; nmlaiki2012@gmail.com (N. Mlaiki)

1. Introduction

Anomalous transport processes, such as subsurface pollutant dispersion or wave attenuation in viscoelastic materials, are common throughout scientific disciplines but cannot be described using classical integer-order models. Time-fractional diffusion-wave equations (TFDWEs) have emerged as an effective structure for describing these complicated phenomena, effectively integrating memory effects and power-law dynamics using fractional-order operators [1–4]. The growth of these operators is vital: from the initial work of Abel, Riemann, and Liouville [5] to the broadly recognized Caputo derivative [6], which added historicity but had a singular kernel. This limitation motivated the development of non-singular alternatives, resulting in the modified Atangana-Baleanu-Caputo (MABC) derivative [7]. The MABC derivative, with its non-singular Mittag-Leffler kernel, provides a more reliable model for systems with complex memory and hereditary properties. The Modified Atangana-Baleanu (MABC) derivative extends the original ABC operator to a wider function space. Crucially, as demonstrated in [7], the MABC derivative can solve a class of fractional differential equations intractable under the standard ABC definition. Its applications span numerous scientific fields, including viscoelasticity [8, 9], control theory [**?**], and biological systems [10–13], with further examples available in the cited literature.

The numerical solution of TFDWEs is a dynamic and challenging area of research. A wide range of approaches has been developed to address these problems, each with its own advantages. Analytical solutions, such as those by Mainardi [14] for 1D cases or Agrawal [15] for bounded domains, provide foundational insights but are impractical for complex, multi-dimensional problems. Therefore, numerical methods have emerged, including finite difference methods (FDM) with compact schemes [16], solvers for multi-term equations [17], and the alternating direction implicit (ADI) method for 2D problems [18]. More advanced techniques, such as meshless techniques [19], spectral methods [20, 21], wavelet-based approaches [22], and hybrid Laplace-spectral methods [23], have further improved spatial accuracy and computational efficiency. These advancements are further exemplified by recent developments such as the Galerkin spectral method with high-order differences [24] and fractional multi-step methods [25], underscoring the rapid progress in the field.

Despite these advances, the non-local nature of fractional operators like the MABC poses a significant computational challenge. Time-stepping methods, including the FDM and spectral methods, suffer significant costs in long-time or high-dimensional simulations due to the need to store and process the entire solution history at each step. This history dependence increases computational cost and complexity, making accurate 3D simulations of anomalous transport processes a significant challenge. While hybrid methods, such as those coupling the LT with a spectral collocation method [23], minimize temporal complexity, a complete framework that fully integrates the time-fractional derivative with rigorous mathematical analysis and demonstrates high performance in a multi-dimensional setting has not yet been developed.

This work addresses this gap by proposing a novel hybrid algorithm that combines the LT with the CSCM. Our approach decouples the temporal and spatial challenges of TFDWEs: the LT transforms the MABC time-fractional operator exactly into the

Laplace domain, eliminating the convolution burden and stability constraints of time-stepping methods. The resulting parameterized Helmholtz-type problems are solved using the CSCM, which achieves exponential convergence in space for smooth solutions [26–28]. The time-domain solution is efficiently recovered using the improved Talbot method for numerical inversion [29]. This approach not only reduces the computational cost but also offers a unified framework for 1D, 2D, and 3D problems.

Beyond computational efficiency, this work provides rigorous mathematical and physical insights. First, we establish a solid theoretical foundation for the MABC-based TFDWE by proving the existence, uniqueness, and Ulam-Hyers stability of its solutions, thereby ensuring the model's well-posedness a critical aspect often overlooked in numerical studies. Furthermore, by eliminating time-stepping, our method facilitates an efficient analysis of how the fractional order α influences solution behavior in multi-dimensional settings, offering new insights into memory effects within complex systems.

The key advantages of the proposed LT-based CSCM approach are threefold. First, it avoids the time-step restrictions and temporal error accumulation inherent in step-wise methods. Second, it efficiently handles the memory effects of the MABC derivative via the Laplace transform while leveraging the CSCM for exponential convergence of smooth spatial solutions. Finally, the method requires fewer discretization nodes for high accuracy compared to other methods, which significantly reduces computational and storage costs and provides a unified framework for solving 1D, 2D, and 3D problems.

The rest of this paper is organized as follows. Section 2 introduces the necessary preliminary definitions. The analysis of existence, uniqueness, and stability is presented in Section 3. Section 4 provides a detailed description of the proposed numerical method. Numerical results for 1D, 2D, and 3D examples are discussed in Section 5, and finally, conclusions are drawn in Section 6.

2. Preliminaries

This section presents the fundamental definitions and mathematical prerequisites for the current study.

Definition 1. *The Laplace transform (LT) of a function $u(\bar{\boldsymbol{x}}, t)$ is defined as:*

$$\mathscr{L}\{\mathrm{u}(\bar{\boldsymbol{x}}, \tau)\} = \widehat{\mathrm{u}}(\bar{\boldsymbol{x}}, s) = \int_0^\infty e^{s\tau}\mathrm{u}(\bar{\boldsymbol{x}}, \tau)d\tau$$

Definition 2. *The MABC derivative of order $0 < \alpha < 1$ of a function $\mathrm{u}(\bar{\boldsymbol{x}}, \tau) \in L^1(0, T)$ in Caputo sense is defined by [30]:*

$$\begin{aligned} {}_0^{MABC}D_\tau^\alpha \mathrm{u}(\bar{\boldsymbol{x}}, \tau) = \frac{\beta(\alpha)}{1-\alpha}\Bigg[&\mathrm{u}(\bar{\boldsymbol{x}}, \tau) - \mathcal{E}_\alpha\left(-\eta_\alpha \tau^\alpha\right)\mathrm{u}(\bar{\boldsymbol{x}}, 0) \\ &- \eta_\alpha \int_0^\tau (\tau-\vartheta)^{\alpha-1}\mathcal{E}_{\alpha,\alpha}\left(-\eta_\alpha(\tau-\vartheta)^\alpha\right)\mathrm{u}(\bar{\boldsymbol{x}}, \vartheta)d\vartheta\Bigg], \end{aligned}$$

Definition 3. *Let* $\mathrm{u}^{(n-1)}(\bar{\boldsymbol{x}},\tau) \in L^1(0,T)$, *then the MABC derivative of order* $n-1 < \alpha_1 < n$ *of a function in Caputo sense is defined by [30]:*

$$
\begin{aligned}
{}_0^{MABC}D_\tau^{\alpha_1}\mathrm{u}(\bar{\boldsymbol{x}},\tau) = \frac{\beta(\alpha)}{1-\alpha}\Bigg[&\mathrm{u}^{(n-1)}(\bar{\boldsymbol{x}},\tau) - \mathcal{E}_\alpha\left(-\eta_\alpha\tau^\alpha\right)\mathrm{u}^{(n-1)}(\bar{\boldsymbol{x}},0)\\
&- \eta_\alpha\int_0^\tau(\tau-\vartheta)^{\alpha-1}\mathcal{E}_{\alpha,\alpha}\left(-\eta_\alpha(\tau-\vartheta)^\alpha\right)\mathrm{u}^{(n-1)}(\bar{\boldsymbol{x}},\vartheta)d\vartheta\Bigg],
\end{aligned}
$$

where $\alpha_1 = \alpha + n - 1$, $\eta_\alpha = \frac{\alpha}{1-\alpha}$, $\beta(\alpha)$ *is a normalized function having the property* $\beta(0) = \beta(1) = 1$, *and* $\mathcal{E}_\alpha(\cdot)$ *is a Mittag-Leffler function defined as*

$$
\mathcal{E}_\alpha(\tau) = \sum_{\ell=0}^{\infty}\frac{\tau^\ell}{\Gamma(\alpha\ell+1)}.
$$

Definition 4. *For* $\mathrm{u}(\bar{\boldsymbol{x}},\tau) \in L^1(0,T)$, *the MABC fractional integral operator is defined by [30]:*

$$
{}_{MABC}\mathfrak{T}_0^\alpha\mathrm{u}(\bar{\boldsymbol{x}},\tau) = \frac{1-\alpha}{\beta(\alpha)}\mathrm{u}(\bar{\boldsymbol{x}},\tau) + \frac{\alpha}{\beta(\alpha)\Gamma(\alpha)}\int_0^\tau(\tau-\vartheta)^\alpha\mathrm{u}(\bar{\boldsymbol{x}},\tau)d\tau,\ \tau \geq 0.
$$

Definition 5. *The LT of MABC derivative of a function* $\mathrm{u}(\bar{\boldsymbol{x}},\tau)$ *is defined by [30]:*

$$
\mathscr{L}\left\{{}_0^{MABC}D_\tau^\alpha\mathrm{u}(\bar{\boldsymbol{x}},\tau)\right\} = \frac{s^\alpha\widehat{\mathrm{u}}(\bar{\boldsymbol{x}},s) - s^{\alpha-1}\widehat{\mathrm{u}}(\bar{\boldsymbol{x}},0)}{s^\alpha(1-\alpha)+\alpha}.
$$

3. Existence and uniqueness results

We establish the existence and uniqueness of the solution to the given problem in this section. We begin by defining an appropriate functional framework: Let $\mathrm{B}(\Omega,\mathbb{R})$ represent the Banach space comprising all continuous real-valued functions defined on the compact domain $\Omega = \Theta \times [0,1]$ where $\Theta \subset \mathbb{R}^3$. The compactness of Ω ensures that $\mathrm{B}(\Omega,\mathbb{R})$ is well suited for studying the continuity and boundedness properties of sections. The norm on $\mathrm{B}(\Omega,\mathbb{R})$ is a supremum norm given by:

$$
\|\mathrm{u}\|_\infty = \sup\{|\mathrm{u}(\bar{\boldsymbol{x}},\tau)| : (\bar{\boldsymbol{x}},\tau) \in \Omega\},
$$

where $\bar{\boldsymbol{x}} \in \Theta$ represents the spatial co ordinates and $\tau \in [0,1]$ denotes the temporal variable. We study the fractional diffusion-wave equation of the form [31]:

$$
{}_0^{MABC}D_\tau^\alpha\mathrm{u}(\bar{\boldsymbol{x}},\tau) = \lambda_1\nabla^2\mathrm{u}(\bar{\boldsymbol{x}},\tau) - \lambda_2\mathrm{u}(\bar{\boldsymbol{x}},\tau) + f(\bar{\boldsymbol{x}},\tau),\ 1 < \alpha \leq 2,\ \bar{\boldsymbol{x}} \in \Theta, \tag{1}
$$

with boundary conditions

$$
\mathcal{B}\mathrm{u}(\bar{\boldsymbol{x}},\tau) = g_1(\bar{\boldsymbol{x}},\tau), \bar{\boldsymbol{x}} \in \partial\Theta, \tag{2}
$$

and initial conditions

$$
\begin{aligned}
&\mathrm{u}(\bar{\boldsymbol{x}},0) = g_2(\bar{\boldsymbol{x}}),\\
&\mathrm{u}_\tau(\bar{\boldsymbol{x}},0) = g_3(\bar{\boldsymbol{x}}),
\end{aligned} \tag{3}
$$

where ∇^2 is the Laplacian operator, defined as: for $1D$ problem, $\bar{\boldsymbol{x}} = x$ and $\nabla^2 = \frac{\partial^2}{\partial x^2}$; for a $2D$ problem, $\bar{\boldsymbol{x}} = (x, y)$ and $\nabla^2 = \frac{\partial^2}{\partial x^2} + \frac{\partial^2}{\partial y^2}$; and for a $3D$ problem, $\bar{\boldsymbol{x}} = (x, y, z)$ and $\nabla^2 = \frac{\partial^2}{\partial x^2} + \frac{\partial^2}{\partial y^2} + \frac{\partial^2}{\partial z^2}$. Here Θ is the domain and $\partial\Theta$ is its boundary. The constants λ_1 and λ_2 are arbitrary, and the forcing term $f(\bar{\boldsymbol{x}}, \tau)$ is sufficiently smooth. The functions $g_1(\bar{\boldsymbol{x}}, \tau)$, $g_2(\bar{\boldsymbol{x}})$, and $g_3(\bar{\boldsymbol{x}})$ are given continuous functions. $\mathcal{B}$ is the boundary differential operator, and ${}_0^{MABC}D_\tau^\alpha u(\bar{\boldsymbol{x}}, \tau)$, denotes the MABC derivative of order $1 < \alpha < 2$. Applying the MABC fractional integral operator to Eq (1), yields:

$$\begin{aligned} \mathrm{u}(\bar{\boldsymbol{x}}, \tau) = g_2(\bar{\boldsymbol{x}}) + g_3(\bar{\boldsymbol{x}})t + \frac{(1-\alpha)}{\beta(\alpha)}\left(\lambda_1 \nabla^2 \mathrm{u}(\bar{\boldsymbol{x}}, \tau) - \lambda_2 \mathrm{u}(\bar{\boldsymbol{x}}, \tau) + f(\bar{\boldsymbol{x}}, \tau)\right) \\ + \frac{\alpha}{\beta(\alpha)\Gamma(\alpha)}\left(\int_0^\tau (\tau - \vartheta)^{\alpha-1}\left(\lambda_1 \nabla^2 \mathrm{u}(\bar{\boldsymbol{x}}, \vartheta) - \lambda_2 \mathrm{u}(\bar{\boldsymbol{x}}, \vartheta) + f(\bar{\boldsymbol{x}}, \vartheta)\right) d\vartheta\right). \end{aligned} \tag{4}$$

Next, we define the operator $\mathcal{J} : \mathrm{B}(\Omega, \mathbb{R}) \to \mathrm{B}(\Omega, \mathbb{R})$, transforming the problem into a fixed-point formulation:

$$\begin{aligned} \mathcal{J}\mathrm{u}(\bar{\boldsymbol{x}}, \tau) = g_2(\bar{\boldsymbol{x}}) + g_3(\bar{\boldsymbol{x}})t + \frac{(1-\alpha)}{\beta(\alpha)}\left(\lambda_1 \nabla^2 \mathrm{u}(\bar{\boldsymbol{x}}, \tau) - \lambda_2 \mathrm{u}(\bar{\boldsymbol{x}}, \tau) + f(\bar{\boldsymbol{x}}, \tau)\right) \\ + \frac{\alpha}{\beta(\alpha)\Gamma(\alpha)}\left(\int_0^\tau (\tau - \vartheta)^{\alpha-1}\left(\lambda_1 \nabla^2 \mathrm{u}(\bar{\boldsymbol{x}}, \vartheta) - \lambda_2 \mathrm{u}(\bar{\boldsymbol{x}}, \vartheta) + f(\bar{\boldsymbol{x}}, \vartheta)\right) d\vartheta\right). \end{aligned} \tag{5}$$

The fixed point of the operator corresponds to the solution to Eqs. (1)–(3). We introduce the following hypotheses for any $(\vartheta, \tau) \in (\Omega)$:

$(\mathbf{H_1})$ $|\nabla^2 \mathrm{u}(\bar{\boldsymbol{x}}, \tau)| \leq \epsilon_1 |\mathrm{u}(\bar{\boldsymbol{x}}, \tau)|$,
$(\mathbf{H_2})$ $|g_2| \leq \epsilon_2$,
$(\mathbf{H_3})$ $|g_3| \leq \epsilon_3$,
$(\mathbf{H_4})$ $|f(\bar{\boldsymbol{x}}, \tau)| \leq \epsilon_4$,
$(\mathbf{H_5})$ $|\nabla^2 \mathrm{u}_1(\bar{\boldsymbol{x}}, \tau) - \nabla^2 \mathrm{u}_2(\bar{\boldsymbol{x}}, \tau)| \leq \epsilon_5 |\mathrm{u}_1(\bar{\boldsymbol{x}}, \tau) - \mathrm{u}_2(\bar{\boldsymbol{x}}, \tau)|$,
$(\mathbf{H_6})$ $|\nabla^2 \mathrm{u}_1(\bar{\boldsymbol{x}}_1, \tau_1) - \nabla^2 \mathrm{u}_2(\bar{\boldsymbol{x}}_2, \tau_2)| \leq \mathcal{L}_{f_1}\left(|\bar{\boldsymbol{x}}_1 - \bar{\boldsymbol{x}}_2| + |\tau_1 - \tau_2||\right)$,
$(\mathbf{H_7})$ $|\mathrm{u}_1(\bar{\boldsymbol{x}}_1, \tau_1) - \mathrm{u}_2(\bar{\boldsymbol{x}}_2, \tau_2)| \leq \mathcal{L}_{f_2}\left(|\bar{\boldsymbol{x}}_1 - \bar{\boldsymbol{x}}_2| + |\tau_1 - \tau_2||\right)$,
$(\mathbf{H_8})$ $|f(\bar{\boldsymbol{x}}_1, \tau_1) - f(\bar{\boldsymbol{x}}_2, \tau_2)| \leq \mathcal{L}_{f_3}\left(|\bar{\boldsymbol{x}}_1 - \bar{\boldsymbol{x}}_2| + |\tau_1 - \tau_2||\right)$,
$(\mathbf{H_9})$ $|g_2(\bar{\boldsymbol{x}}_1) - g_2(\bar{\boldsymbol{x}}_2)| \leq \mathcal{L}_{g_2}|\bar{\boldsymbol{x}}_1 - \bar{\boldsymbol{x}}_2| \leq \mathcal{L}_{g_2}\delta_1$,
$(\mathbf{H_{10}})$ $|g_3(\bar{\boldsymbol{x}}_1) - g_3(\bar{\boldsymbol{x}}_2)| \leq \mathcal{L}_{g_3}|\bar{\boldsymbol{x}}_1 - \bar{\boldsymbol{x}}_2| \leq \mathcal{L}_{g_3}\delta_1$,

where $\epsilon_1, \epsilon_2, \epsilon_3, \epsilon_4, \epsilon_5, \mathcal{L}_{f_1}, \mathcal{L}_{f_2}, \mathcal{L}_{f_3}, \mathcal{L}_{g_2}, \mathcal{L}_{g_3} > 0$ are constants.

The problem defined by Eqs. (1)–(3) has at least one solution.

Proof. The proof proceeds in several steps. We apply the Schaefer fixed-point theorem to establish the existence of a solution.

Step 1: In the first we show that the operator $\mathcal{J}$ is continuous. Consider a sequence

$\mathrm{u}_m \to \mathrm{u}$ in $\mathrm{B}(\Omega, \mathbb{R})$. For $(\bar{\boldsymbol{x}}, \tau) \in \Omega$, we compute:

$$\begin{aligned}
&\|\mathcal{J}\mathrm{u}_m(\bar{\boldsymbol{x}},\tau) - \mathcal{J}\mathrm{u}(\bar{\boldsymbol{x}},\tau)\|_\infty = \sup_{(\bar{\boldsymbol{x}},\tau)\in\Omega}\left\{|\mathcal{J}\mathrm{u}_m(\bar{\boldsymbol{x}},\tau) - \mathcal{J}\mathrm{u}(\bar{\boldsymbol{x}},\tau)|\right\}\\
=&\sup_{(\bar{\boldsymbol{x}},\tau)\in\Omega}\left\{\left|\frac{1-\alpha}{\beta(\alpha)}\Big(\lambda_1\nabla^2\mathrm{u}_m(\bar{\boldsymbol{x}},\tau) - \lambda_2\mathrm{u}_m(\bar{\boldsymbol{x}},\tau)\Big) + \frac{\alpha}{\Gamma(\alpha)\beta(\alpha)}\int_0^\tau(\tau-\vartheta)^{\alpha-1}\Big(\lambda_1\nabla^2\mathrm{u}_m(\bar{\boldsymbol{x}},\vartheta) - \lambda_2\mathrm{u}_m(\bar{\boldsymbol{x}},\vartheta)\Big)d\vartheta\right.\\
&\left.-\frac{1-\alpha}{\beta(\alpha)}\Big(\lambda_1\nabla^2\mathrm{u}(\bar{\boldsymbol{x}},\tau) - \lambda_2\mathrm{u}(\bar{\boldsymbol{x}},\tau)\Big) - \frac{\alpha}{\Gamma(\alpha)\beta(\alpha)}\int_0^\tau(\tau-\vartheta)^{\alpha-1}\Big(\lambda_1\nabla^2\mathrm{u}(\bar{\boldsymbol{x}},\vartheta) - \lambda_2\mathrm{u}(\bar{\boldsymbol{x}},\vartheta)\Big)d\vartheta\right|\Bigg\}\\
\le&\sup_{(\bar{\boldsymbol{x}},\tau)\in\Omega}\left\{\frac{1-\alpha}{\beta(\alpha)}\Big(|\lambda_1||\nabla^2\mathrm{u}_m(\bar{\boldsymbol{x}},\tau) - \nabla^2\mathrm{u}(\bar{\boldsymbol{x}},\tau)| + |\lambda_2||\mathrm{u}_m(\bar{\boldsymbol{x}},\tau) - \mathrm{u}(\bar{\boldsymbol{x}},\tau)|\Big)\right.\\
&\left.-\frac{\alpha}{\Gamma(\alpha)\beta(\alpha)}\int_0^\tau(\tau-\vartheta)^{\alpha-1}\Big(|\lambda_1||\nabla^2\mathrm{u}_m(\bar{\boldsymbol{x}},\vartheta) - \nabla^2\mathrm{u}(\bar{\boldsymbol{x}},\vartheta)| + |\lambda_2||\mathrm{u}_m(\bar{\boldsymbol{x}},\vartheta) - \mathrm{u}(\bar{\boldsymbol{x}},\vartheta)|\Big)d\vartheta.\right\}
\end{aligned}$$

Using hypotheses $\mathbf{H_5}$, we have

$$\begin{aligned}
&\|\mathcal{J}\mathrm{u}_m(\bar{\boldsymbol{x}},\tau) - \mathcal{J}\mathrm{u}(\bar{\boldsymbol{x}},\tau)\|_\infty \le \sup_{(\bar{\boldsymbol{x}},\tau)\in\Omega}\left\{\frac{1-\alpha}{\beta(\alpha)}\Big(|\lambda_1|\epsilon_5|\mathrm{u}_m(\bar{\boldsymbol{x}},\tau) - \mathrm{u}(\bar{\boldsymbol{x}},\tau)| + |\lambda_2||\mathrm{u}_m(\bar{\boldsymbol{x}},\tau) - \mathrm{u}(\bar{\boldsymbol{x}},\tau)|\Big)\right.\\
&\left.+\frac{\alpha}{\Gamma(\alpha)\beta(\alpha)}\int_0^\tau(\tau-\vartheta)^{\alpha-1}\Big(\epsilon_5|\lambda_1||\mathrm{u}_m(\bar{\boldsymbol{x}},\vartheta) - \mathrm{u}(\bar{\boldsymbol{x}},\vartheta)| + |\lambda_2||\mathrm{u}_m(\bar{\boldsymbol{x}},\vartheta) - \mathrm{u}(\bar{\boldsymbol{x}},\vartheta)|\Big)d\vartheta\right\}\\
\le&\frac{1-\alpha}{\beta(\alpha)}\Big((|\lambda_1|\epsilon_5 + |\lambda_2|)\|\mathrm{u}_m - \mathrm{u}\|_\infty\Big) + \frac{\alpha}{\Gamma(\alpha)\beta(\alpha)}\int_0^\tau(\tau-\vartheta)^{\alpha-1}\Big((\epsilon_5|\lambda_1| + |\lambda_2|)\|\mathrm{u}_m - \mathrm{u}\|_\infty\Big)d\vartheta\\
=&\frac{1-\alpha}{\beta(\alpha)}\Big((|\lambda_1|\epsilon_5 + |\lambda_2|)\|\mathrm{u}_m - \mathrm{u}\|_\infty\Big) + \frac{\tau^\alpha}{\Gamma(\alpha)\beta(\alpha)}\Big((\epsilon_5|\lambda_1| + |\lambda_2|)\|\mathrm{u}_m - \mathrm{u}\|_\infty\Big)\\
=&\frac{(1-\alpha)\Gamma(\alpha) + \tau^\alpha}{\Gamma(\alpha)\beta(\alpha)}\Big((|\lambda_1|\epsilon_5 + |\lambda_2|)\|\mathrm{u}_m - \mathrm{u}\|_\infty\Big)
\end{aligned}$$

Since $\mathrm{u}_m \to \mathrm{u}$ in $\mathrm{B}(\Omega, \mathbb{R})$, we have$\|\mathrm{u}_m - \mathrm{u}\|_\infty \to 0$, as $m \to \infty$. Hence, $\|\mathcal{J}\mathrm{u}_m - \mathcal{J}\mathrm{u}\|_\infty \to 0$, proving that $\mathcal{J}$ is continuous.

Step 2: Boundedness of $\mathcal{J}$. Let $R_\gamma = \{\mathrm{u} \in C(\Lambda, \mathbb{R}) : \|\mathrm{u}\|_\infty \le \gamma\}$ for some $\gamma > 0$. For $\mathrm{u} \in R_\gamma$, we estimate:

$$\begin{aligned}
|\mathcal{J}\mathrm{u}(\bar{\boldsymbol{x}},\tau)| =&\left|g_2(\bar{\boldsymbol{x}}) + g_3(\bar{\boldsymbol{x}})\tau + \frac{1-\alpha}{\beta(\alpha)}\Big(\lambda_1\nabla^2\mathrm{u}(\bar{\boldsymbol{x}},\tau) - \lambda_2\mathrm{u}(\bar{\boldsymbol{x}},\tau) + f(\bar{\boldsymbol{x}},\tau)\Big)\right.\\
&\left.+\frac{\alpha}{\Gamma(\alpha)\beta(\alpha)}\int_0^\tau(\tau-\vartheta)^{\alpha-1}\Big(\lambda_1\nabla^2\mathrm{u}(\bar{\boldsymbol{x}},\vartheta) - \lambda_2\mathrm{u}(\bar{\boldsymbol{x}},\vartheta) + f(\bar{\boldsymbol{x}},\vartheta)\Big)d\vartheta\right|\\
\le&|g_2(\bar{\boldsymbol{x}})| + |g_3(\bar{\boldsymbol{x}})|\tau + \frac{1-\alpha}{\beta(\alpha)}\Big(|\lambda_1||\nabla^2\mathrm{u}(\bar{\boldsymbol{x}},\tau)| + |\lambda_2||\mathrm{u}(\bar{\boldsymbol{x}},\tau)| + |f(\bar{\boldsymbol{x}},\tau)|\Big)\\
&+\frac{\alpha}{\Gamma(\alpha)\beta(\alpha)}\int_0^\tau(\tau-\vartheta)^{\alpha-1}\Big(|\lambda_1||\nabla^2\mathrm{u}(\bar{\boldsymbol{x}},\vartheta)| + |\lambda_2||\mathrm{u}(\bar{\boldsymbol{x}},\vartheta)| + |f(\bar{\boldsymbol{x}},\vartheta)|\Big)d\vartheta\Big|.
\end{aligned}$$

Using $\mathbf{H_1} - \mathbf{H_4}$, we have

$$|\mathcal{J}\mathrm{u}(\bar{\boldsymbol{x}},\tau)| \leq \epsilon_2 + \tau\epsilon_3 + \frac{1-\alpha}{\beta(\alpha)}\Big(|\lambda_1|\epsilon_1|\mathrm{u}(\bar{\boldsymbol{x}},\tau)| + |\lambda_2||\mathrm{u}(\bar{\boldsymbol{x}},\tau)| + \epsilon_4\Big)$$
$$+ \frac{\alpha}{\Gamma(\alpha)\beta(\alpha)}\int_0^{\tau}(\tau-\vartheta)^{\alpha-1}\Big(|\lambda_1|\epsilon_1|\mathrm{u}(\bar{\boldsymbol{x}},\vartheta)| + |\lambda_2||\mathrm{u}(\bar{\boldsymbol{x}},\vartheta)| + \epsilon_4\Big)d\vartheta\Big|$$

or

$$\begin{aligned}\|\mathcal{J}\mathrm{u}\|_\infty \leq& \epsilon_2 + \tau\epsilon_3 + \frac{1-\alpha}{\beta(\alpha)}\Big(|\lambda_1|\epsilon_1\|\mathrm{u}\|_\infty + |\lambda_2|\|\mathrm{u}\|_\infty + \epsilon_4\Big)\\ &+ \frac{\alpha}{\Gamma(\alpha)\beta(\alpha)}\int_0^{\tau}(\tau-\vartheta)^{\alpha-1}\Big(|\lambda_1|\epsilon_1\|\mathrm{u}\|_\infty + |\lambda_2|\|\mathrm{u}\|_\infty + \epsilon_4\Big)d\vartheta\Big|\\ &= \epsilon_2 + \tau\epsilon_3 + \frac{\Gamma(\alpha)(1-\alpha)+\tau^\alpha}{\Gamma(\alpha)\beta(\alpha)}\Big(|\lambda_1|\epsilon_1\|\mathrm{u}\|_\infty + |\lambda_2|\|\mathrm{u}\|_\infty + \epsilon_4\Big)\\ &\leq \epsilon_2 + \tau\epsilon_3 + \frac{\Gamma(\alpha)(1-\alpha)+\tau^\alpha}{\Gamma(\alpha)\beta(\alpha)}\Big(|\lambda_1|\epsilon_1\gamma + |\lambda_2|\gamma + \epsilon_4\Big),\end{aligned}$$

since $\tau \in [0,1]$, we have

$$\|\mathcal{J} \leq \mathrm{u}\|_\infty \leq \epsilon_2 + \epsilon_3 + \frac{\Gamma(\alpha)(1-\alpha)+1}{\Gamma(\alpha)\beta(\alpha)}\Big(|\lambda_1|\epsilon_1\gamma + |\lambda_2|\gamma + \epsilon_4\Big) =: \rho_{ab},$$

where ρ_{ab} is a constant independent of u. Thus, $\mathcal{J}$ is bounded.

Step 3: Equicontinuity of $\mathcal{J}$. Let $\mathrm{u} \in R_\gamma$ and $(\bar{\boldsymbol{x}}_1,\tau_1),(\bar{\boldsymbol{x}}_2,\tau_2) \in \Omega$ with $\|\bar{\boldsymbol{x}}_1-\bar{\boldsymbol{x}}_2\| < \delta_1$ and $|\tau_1-\tau_2| < \delta_2$. We analyze:

$$\begin{aligned}&|\mathcal{J}\mathrm{u}(\bar{\boldsymbol{x}}_1,\tau_1) - \mathcal{J}\mathrm{u}(\bar{\boldsymbol{x}}_2,\tau_2)| \leq |g_2(\bar{\boldsymbol{x}}_1) - g_2(\bar{\boldsymbol{x}}_2)| + |g_3(\bar{\boldsymbol{x}}_1) - g_3(\bar{\boldsymbol{x}}_2)|\tau_1 + |g_3(\bar{\boldsymbol{x}}_2)||\tau_1-\tau_2|\\ &+ \frac{1-\alpha}{\beta(\alpha)}\Big|\lambda_1\nabla^2\mathrm{u}(\bar{\boldsymbol{x}}_1,\tau_1) - \lambda_1\nabla^2\mathrm{u}(\bar{\boldsymbol{x}}_2,\tau_2) + \lambda_2\mathrm{u}(\bar{\boldsymbol{x}}_2,\tau_2) - \lambda_2\mathrm{u}(\bar{\boldsymbol{x}}_1,\tau_1) + f(\bar{\boldsymbol{x}}_1,\tau_1) - f(\bar{\boldsymbol{x}}_2,\tau_2)\Big|\\ &+ \frac{\alpha}{\Gamma(\alpha)\beta(\alpha)}\Big|\int_0^{\tau_1}(\tau_1-\vartheta)^{\alpha-1}\Big(\lambda_1\nabla^2\mathrm{u}(\bar{\boldsymbol{x}}_1,\vartheta) - \lambda_2\mathrm{u}(\bar{\boldsymbol{x}}_1,\vartheta) + f(\bar{\boldsymbol{x}}_1,\vartheta)\Big)d\vartheta\\ &- \int_0^{\tau_2}(\tau_2-\vartheta)^{\alpha-1}\Big(\lambda_1\nabla^2\mathrm{u}(\bar{\boldsymbol{x}}_2,\vartheta) - \lambda_2\mathrm{u}(\bar{\boldsymbol{x}}_2,\vartheta) + f(\bar{\boldsymbol{x}}_2,\vartheta)\Big)d\vartheta\Big|\end{aligned}$$

Using $\mathbf{H_3}$ and $\mathbf{H_6} - \mathbf{H_{10}}$, we have

$$\begin{aligned}&|\mathcal{J}\mathrm{u}(\bar{\boldsymbol{x}}_1,\tau_1) - \mathcal{J}\mathrm{u}(\bar{\boldsymbol{x}}_2,\tau_2)| \leq \mathcal{L}_{g_2}\delta_1 + \mathcal{L}_{g_3}\delta_1 + \epsilon_3\delta_2 + \frac{1-\alpha}{\beta(\alpha)}\left(|\lambda_1|\mathcal{L}_{f_1}\left(|\bar{\boldsymbol{x}}_1-\bar{\boldsymbol{x}}_2| + |\tau_1-\tau_2|\right)\right) + |\lambda_2|\mathcal{L}_{f_2}\left(|\bar{\boldsymbol{x}}_1-\bar{\boldsymbol{x}}_2|\right.\\ &\left.+|\tau_1-\tau_2|\right) + \mathcal{L}_{f_3}\left(|\bar{\boldsymbol{x}}_1-\bar{\boldsymbol{x}}_2| + |\tau_1-\tau_2|\right))\\ &+ \frac{\alpha}{\Gamma(\alpha)\beta(\alpha)}\Big|\int_0^{\tau_1}(\tau_1-\vartheta)^{\alpha-1}\Big(\lambda_1\nabla^2\mathrm{u}(\bar{\boldsymbol{x}}_1,\vartheta) - \lambda_2\mathrm{u}(\bar{\boldsymbol{x}}_1,\vartheta) + f(\bar{\boldsymbol{x}}_1,\vartheta)\Big)d\vartheta\\ &- \int_0^{\tau_2}(\tau_2-\vartheta)^{\alpha-1}\Big(\lambda_1\nabla^2\mathrm{u}(\bar{\boldsymbol{x}}_2,\vartheta) - \lambda_2\mathrm{u}(\bar{\boldsymbol{x}}_2,\vartheta) + f(\bar{\boldsymbol{x}}_2,\vartheta)\Big)d\vartheta\Big|,\end{aligned}$$

Next, we split the difference of integrals into three parts as follows:

$$\begin{aligned}
&\Big| \int_0^{\tau_1} (\tau_1-\vartheta)^{\alpha-1}\Big(\lambda_1\nabla^2\mathrm{u}(\bar{\boldsymbol{x}}_1,\vartheta)-\lambda_2\mathrm{u}(\bar{\boldsymbol{x}}_1,\vartheta)+f(\bar{\boldsymbol{x}}_1,\vartheta)\Big)d\vartheta \\
&\quad - \int_0^{\tau_2} (\tau_2-\vartheta)^{\alpha-1}\Big(\lambda_1\nabla^2\mathrm{u}(\bar{\boldsymbol{x}}_2,\vartheta)-\lambda_2\mathrm{u}(\bar{\boldsymbol{x}}_2,\vartheta)+f(\bar{\boldsymbol{x}}_2,\vartheta)\Big)d\vartheta\Big| \\
&= \Big[\underbrace{\int_0^{\tau_1} \left[(\tau_1-\vartheta)^{\alpha-1}-(\tau_2-\vartheta)^{\alpha-1}\right]\Big(\lambda_1\nabla^2\mathrm{u}(\bar{\boldsymbol{x}}_1,\vartheta)-\lambda_2\mathrm{u}(\bar{\boldsymbol{x}}_1,\vartheta)+f(\bar{\boldsymbol{x}}_1,\vartheta)\Big)d\vartheta}_{\text{(i)}} \\
&\quad + \underbrace{\int_0^{\tau_1} (\tau_2-\vartheta)^{\alpha-1}\Big(\lambda_1[\nabla^2\mathrm{u}(\bar{\boldsymbol{x}}_1,\vartheta)-\nabla^2\mathrm{u}(\bar{\boldsymbol{x}}_2,\vartheta)]-\lambda_2[\mathrm{u}(\bar{\boldsymbol{x}}_1,\vartheta)-\mathrm{u}(\bar{\boldsymbol{x}}_2,\vartheta)]+[f(\bar{\boldsymbol{x}}_1,\vartheta)-f(\bar{\boldsymbol{x}}_2,\vartheta)]\Big)d\vartheta}_{\text{(ii)}} \\
&\quad + \underbrace{\int_{\tau_1}^{\tau_2} (\tau_2-\vartheta)^{\alpha-1}\Big(\lambda_1\nabla^2\mathrm{u}(\bar{\boldsymbol{x}}_2,\vartheta)-\lambda_2\mathrm{u}(\bar{\boldsymbol{x}}_2,\vartheta)+f(\bar{\boldsymbol{x}}_2,\vartheta)\Big)d\vartheta}_{\text{(iii)}}\Big]
\end{aligned}$$

for the integral (i), using the mean value theorem, we have

$$|(\tau_1-\vartheta)^{\alpha-1}-(\tau_2-\vartheta)^{\alpha-1}| \le (\alpha-1)(\tau_2-\tau_1)(\tau_1-\vartheta)^{\alpha-2}$$

Therefore:

$$\begin{aligned}
\text{(i)} &\le (\lambda_1\|\nabla^2\mathrm{u}\|_\infty+\lambda_2\|\mathrm{u}\|_\infty+\|f\|_\infty)(\alpha-1)\delta_2\int_0^{\tau_1}(\tau_1-\vartheta)^{\alpha-2}d\vartheta \\
&= (\lambda_1\|\nabla^2\mathrm{u}\|_\infty+\lambda_2\|\mathrm{u}\|_\infty+\|f\|_\infty)\delta_2\tau_1^{\alpha-1}.
\end{aligned}$$

Similarly, using Lipschitz conditions for integral (ii), we have:

$$\begin{aligned}
\text{(ii)} &\le (\lambda_1\mathcal{L}_{f_1}+\lambda_2\mathcal{L}_{f_2}+\mathcal{L}_{f_3})\delta_1\int_0^{\tau_1}(\tau_2-\vartheta)^{\alpha-1}d\vartheta \\
&= (\lambda_1\mathcal{L}_{f_1}+\lambda_2\mathcal{L}_{f_2}+\mathcal{L}_{f_3})\delta_1\big(\frac{\tau_2^\alpha}{\alpha}-\frac{\delta_2}{\alpha}\big).
\end{aligned}$$

and using direct estimation, we have:

$$\begin{aligned}
\text{(iii)} &\le (\lambda_1\|\nabla^2\mathrm{u}\|_\infty+\lambda_2\|\mathrm{u}\|_\infty+\|f\|_\infty)\int_{\tau_1}^{\tau_2}(\tau_2-\vartheta)^{\alpha-1}d\vartheta \\
&= (\lambda_1\|\nabla^2\mathrm{u}\|_\infty+\lambda_2\|\mathrm{u}\|_\infty+\|f\|_\infty)\frac{\delta_2}{\alpha}.
\end{aligned}$$

Combining all the results, we obtain:

$$\|\mathcal{J}\mathrm{u}(\bar{\boldsymbol{x}}_1,\tau_1)-\mathcal{J}\mathrm{u}(\bar{\boldsymbol{x}}_2,\tau_2)\|_\infty \le \mathcal{L}_{g_2}\delta_1+\mathcal{L}_{g_3}\delta_1+\epsilon_3\delta_2+\frac{1-\alpha}{\beta(\alpha)}\Bigg(|\lambda_1|\mathcal{L}_{f_1}(\delta_1+\delta_2)+|\lambda_2|\mathcal{L}_{f_2}(\delta_1+\delta_2)$$
$$+\mathcal{L}_{f_3}(\delta_1+\delta_2)\Bigg)+\frac{\alpha}{\Gamma(\alpha)\beta(\alpha)}\Bigg((\lambda_1\|\nabla^2\mathrm{u}\|_\infty+\lambda_2\|\mathrm{u}\|_\infty+\|f\|_\infty)\delta_2\tau_1^{\alpha-1}+(\lambda_1\mathcal{L}_{f_1}+\lambda_2\mathcal{L}_{f_2}+\mathcal{L}_{f_3})\delta_1\big(\frac{\tau_2^\alpha}{\alpha}-\frac{\delta_2}{\alpha}\big)$$
$$+(\lambda_1\|\nabla^2\mathrm{u}\|_\infty+\lambda_2\|\mathrm{u}\|_\infty+\|f\|_\infty)\frac{\delta_2}{\alpha}\Bigg).$$

Hence

$$\|\mathcal{J}\mathrm{u}(\bar{\boldsymbol{x}}_1,\tau_1)-\mathcal{J}\mathrm{u}(\bar{\boldsymbol{x}}_2,\tau_2)\|_\infty \to 0$$

as $\delta_1,\delta_2\to 0$, proving equicontinuity.

Step 4: A Priori Bound. Define $\aleph=\{\mathrm{u}\in \mathrm{B}(\Omega,\mathbb{R}):\mathrm{u}=\varepsilon\mathcal{J}\mathrm{u},\varepsilon\in(0,1)\}$. For $\mathrm{u}\in\aleph$, we have

$$|\mathrm{u}|=|\varepsilon\mathcal{J}\mathrm{u}|=\varepsilon|\mathcal{J}\mathrm{u}|\le\varepsilon\rho_{ab},$$

where ρ_{ab} is defined as in Step 2. The inequality $\|\mathrm{u}\|_\infty\le\rho_{ab}$ implies the operator $\aleph$ is bounded. Therefore, by the Schaefer fixed-point theorem [32], $\mathcal{J}$ has at least one fixed point, ensuring the existence of a solution to the problem.

The problem defined in Eq. (1) has a unique solution if the following condition is satisfied:

$$\frac{(1-\alpha)\Gamma(\alpha)+\tau^\alpha}{\Gamma(\alpha)\beta(\alpha)}\Bigg(\big(\epsilon_5|\lambda_1|+|\lambda_2|\big)\|\mathrm{u}_1-\mathrm{u}_2\|_\infty\Bigg)<1. \tag{6}$$

Proof.

$$
\begin{aligned}
&\|\mathcal{J}\mathrm{u}_1(\bar{\boldsymbol{x}},\tau)-\mathcal{J}\mathrm{u}_2(\bar{\boldsymbol{x}},\tau)\|_\infty=\sup\Big\{|\mathcal{J}\mathrm{u}_1(\bar{\boldsymbol{x}},\tau)-\mathcal{J}\mathrm{u}_2(\bar{\boldsymbol{x}},\tau)|\Big\}\\
&=\sup\Bigg\{\Bigg|\frac{1-\sigma}{\beta(\alpha)}\Big(\lambda_1\nabla^2\mathrm{u}_1(\bar{\boldsymbol{x}},\tau)-\lambda_2\mathrm{u}_1(\bar{\boldsymbol{x}},\tau)\Big)+\frac{\sigma}{\Gamma(\alpha)\beta(\alpha)}\int_0^\tau(\tau-\vartheta)^{\alpha-1}\Big(\lambda_1\nabla^2\mathrm{u}_1(\bar{\boldsymbol{x}},\vartheta)-\lambda_2\mathrm{u}_1(\bar{\boldsymbol{x}},\vartheta)\Big)d\vartheta\\
&-\frac{1-\alpha}{\beta(\alpha)}\Big(\lambda_1\nabla^2\mathrm{u}_2(\bar{\boldsymbol{x}},\vartheta)-\lambda_2\mathrm{u}_2(\bar{\boldsymbol{x}},\vartheta)\Big)-\frac{\alpha}{\Gamma(\alpha)\beta(\alpha)}\int_0^\tau(\tau-\vartheta)^{\alpha-1}\Big(\lambda_1\nabla^2\mathrm{u}_2(\bar{\boldsymbol{x}},\vartheta)-\lambda_2\mathrm{u}_2(\bar{\boldsymbol{x}},\vartheta)\Big)d\vartheta\Bigg|\Bigg\}\\
&\leq\sup\Bigg\{\frac{1-\alpha}{\beta(\alpha)}\Big(|\lambda_1||\nabla^2\mathrm{u}_1(\bar{\boldsymbol{x}},\tau)-\nabla^2\mathrm{u}_2(\bar{\boldsymbol{x}},\tau)|+|\lambda_2||\mathrm{u}_1(\bar{\boldsymbol{x}},\tau)-\mathrm{u}_2(\bar{\boldsymbol{x}},\tau)|\Big)\\
&-\frac{\alpha}{\Gamma(\alpha)\beta(\alpha)}\int_0^\tau(\tau-\vartheta)^{\alpha-1}\Big(|\lambda_1||\nabla^2\mathrm{u}_1(\bar{\boldsymbol{x}},\vartheta)-\nabla^2\mathrm{u}_2(\bar{\boldsymbol{x}},\vartheta)|+|\lambda_2||\mathrm{u}_1(\bar{\boldsymbol{x}},\vartheta)-\mathrm{u}_2(\bar{\boldsymbol{x}},\vartheta)|\Big)d\vartheta\Bigg\}\\
&\leq\sup\Bigg\{\frac{1-\alpha}{\beta(\alpha)}\Big(\epsilon_5|\lambda_1||\mathrm{u}_1(\bar{\boldsymbol{x}},\tau)-\mathrm{u}_2(\bar{\boldsymbol{x}},\tau)|+|\lambda_2||\mathrm{u}_1(\bar{\boldsymbol{x}},\tau)-\mathrm{u}_2(\bar{\boldsymbol{x}},\tau)|\Big)\\
&+\frac{\alpha}{\Gamma(\alpha)\beta(\alpha)}\int_0^\tau(\tau-\vartheta)^{\alpha-1}\Big(\epsilon_5|\lambda_1||\mathrm{u}_1(\bar{\boldsymbol{x}},\tau)-\mathrm{u}_2(\bar{\boldsymbol{x}},\tau)|+|\lambda_2||\mathrm{u}_1(\bar{\boldsymbol{x}},\tau)-\mathrm{u}_2(\bar{\boldsymbol{x}},\tau)|\Big)d\vartheta\Bigg\}\\
&=\frac{1-\alpha}{\beta(\alpha)}\Big(\big(\epsilon_5|\lambda_1|+|\lambda_2|\big)\|\mathrm{u}_1-\mathrm{u}_2\|_\infty\Big)+\frac{\alpha}{\Gamma(\alpha)\beta(\alpha)}\int_0^\tau(\tau-\vartheta)^{\alpha-1}\Big(\big(\epsilon_5|\lambda_1|+|\lambda_2|\big)\|\mathrm{u}_1-\mathrm{u}_2\|_\infty\Big)d\vartheta\\
&=\frac{(1-\alpha)\Gamma(\alpha)+\tau^\alpha}{\Gamma(\alpha)\beta(\alpha)}\Big(\big(\epsilon_5|\lambda_1|+|\lambda_2|\big)\|\mathrm{u}_1-\mathrm{u}_2\|_\infty\Big).
\end{aligned}
$$

If condition (6) holds, then the operator $\mathcal{J}$ is a contraction. By the Banach fixed-point theorem [32], this implies that $\mathcal{J}$ admits a unique fixed point, which in turn implies that problem (1) has a unique solution.

4. Ulam-Hyers stability

The solution of problem (1)–(3) is Ulam-Hyers stable under hypotheses $\mathbf{H_5}$.

Proof. Let the exact solution of the problem is given by:

$$
\begin{aligned}
\mathrm{u}(\bar{\boldsymbol{x}},\tau)&=g_2(\bar{\boldsymbol{x}})+g_3(\bar{\boldsymbol{x}})t+\frac{(1-\alpha)}{\beta(\alpha)}\left(\lambda_1\nabla^2\mathrm{u}(\bar{\boldsymbol{x}},\tau)+\lambda_2\mathrm{u}(\bar{\boldsymbol{x}},\tau)+f(\bar{\boldsymbol{x}},\tau)\right)\\
&+\frac{\alpha}{\beta(\alpha)\Gamma(\alpha)}\left(\int_0^\tau(\tau-\vartheta)^{\alpha-1}\left(\lambda_1\nabla^2\mathrm{u}(\bar{\boldsymbol{x}},\vartheta)+\lambda_2\mathrm{u}(\bar{\boldsymbol{x}},\vartheta)+f(\bar{\boldsymbol{x}},\vartheta)\right)d\vartheta\right),
\end{aligned}
\tag{7}
$$

and let $\overline{\mathrm{u}}(\bar{\boldsymbol{x}},\tau)$ be the approximate solution defined as:

$$
\begin{aligned}
\overline{\mathrm{u}}(\bar{\boldsymbol{x}},\tau)&=g_2(\bar{\boldsymbol{x}})+g_3(\bar{\boldsymbol{x}})t+\frac{(1-\alpha)}{\beta(\alpha)}\left(\lambda_1\nabla^2\overline{\mathrm{u}}(\bar{\boldsymbol{x}},\tau)+\lambda_2\overline{\mathrm{u}}(\bar{\boldsymbol{x}},\tau)+f(\bar{\boldsymbol{x}},\tau)\right)\\
&+\frac{\alpha}{\beta(\alpha)\Gamma(\alpha)}\left(\int_0^\tau(\tau-\vartheta)^{\alpha-1}\left(\lambda_1\nabla^2\overline{\mathrm{u}}(\bar{\boldsymbol{x}},\vartheta)+\lambda_2\overline{\mathrm{u}}(\bar{\boldsymbol{x}},\vartheta)+f(\bar{\boldsymbol{x}},\vartheta)+\mathcal{F}(\bar{\boldsymbol{x}},\vartheta)\right)d\vartheta\right),
\end{aligned}
\tag{8}
$$

where $\mathcal{F}(\bar{\boldsymbol{x}},\vartheta)$ is a perturbation term with $|\mathcal{F}(\bar{\boldsymbol{x}},\vartheta)| \leq \epsilon_7$ for some constant $\epsilon_7 > 0$. Subtracting (8) from (7), we get:

$$\begin{aligned}
|\mathrm{u}(\bar{\boldsymbol{x}},\tau) - \overline{\mathrm{u}}(\bar{\boldsymbol{x}},\tau)| &= \Bigg| \Bigg(g_2(\bar{\boldsymbol{x}}) + g_3(\bar{\boldsymbol{x}})t + \frac{(1-\alpha)}{\beta(\alpha)} \left(\lambda_1 \nabla^2 \mathrm{u}(\bar{\boldsymbol{x}},\tau) + \lambda_2 \mathrm{u}(\bar{\boldsymbol{x}},\tau) + f(\bar{\boldsymbol{x}},\tau)\right) \\
&\quad + \frac{\alpha}{\beta(\alpha)\Gamma(\alpha)} \left(\int_0^\tau (\tau-\vartheta)^{\alpha-1} \left(\lambda_1 \nabla^2 \mathrm{u}(\bar{\boldsymbol{x}},\vartheta) + \lambda_2 \mathrm{u}(\bar{\boldsymbol{x}},\vartheta) + f(\bar{\boldsymbol{x}},\vartheta)\right) d\vartheta \right) \Bigg) \\
&\quad - \Bigg(g_2(\bar{\boldsymbol{x}}) + g_3(\bar{\boldsymbol{x}})t + \frac{(1-\alpha)}{\beta(\alpha)} \left(\lambda_1 \nabla^2 \overline{\mathrm{u}}(\bar{\boldsymbol{x}},\tau) + \lambda_2 \overline{\mathrm{u}}(\bar{\boldsymbol{x}},\tau) + f(\bar{\boldsymbol{x}},\tau)\right) \\
&\quad + \frac{\alpha}{\beta(\alpha)\Gamma(\alpha)} \left(\int_0^\tau (\tau-\vartheta)^{\alpha-1} \left(\lambda_1 \nabla^2 \overline{\mathrm{u}}(\bar{\boldsymbol{x}},\vartheta) + \lambda_2 \overline{\mathrm{u}}(\bar{\boldsymbol{x}},\vartheta) + f(\bar{\boldsymbol{x}},\vartheta) + \mathcal{F}(\bar{\boldsymbol{x}},\vartheta)\right) d\vartheta \right) \Bigg) \Bigg| \\
&\leq \frac{(1-\alpha)}{\beta(\alpha)} \left(|\lambda_1| |\nabla^2 \mathrm{u}(\bar{\boldsymbol{x}},\tau) - \nabla^2 \overline{\mathrm{u}}(\bar{\boldsymbol{x}},\tau)| + |\lambda_2| |\mathrm{u}(\bar{\boldsymbol{x}},\tau) - \overline{\mathrm{u}}(\bar{\boldsymbol{x}},\tau)| \right) \\
&\quad + \frac{\alpha}{\beta(\alpha)\Gamma(\alpha)} \int_0^\tau (\tau-\vartheta)^{\alpha-1} \left(|\lambda_1| |\nabla^2 \mathrm{u}(\bar{\boldsymbol{x}},\tau) - \nabla^2 \overline{\mathrm{u}}(\bar{\boldsymbol{x}},\tau)| + |\lambda_2| |\mathrm{u}(\bar{\boldsymbol{x}},\tau) - \overline{\mathrm{u}}(\bar{\boldsymbol{x}},\tau)| \right. \\
&\quad \left. + |\mathcal{F}(\bar{\boldsymbol{x}},\tau)| \right) d\vartheta \\
&\leq \frac{(1-\alpha)}{\beta(\alpha)} \left(|\lambda_1| \epsilon_5 |\mathrm{u}(\bar{\boldsymbol{x}},\tau) - \overline{\mathrm{u}}(\bar{\boldsymbol{x}},\tau)| + |\lambda_2| |\mathrm{u}(\bar{\boldsymbol{x}},\tau) - \overline{\mathrm{u}}(\bar{\boldsymbol{x}},\tau)| \right) \\
&\quad + \frac{\alpha}{\beta(\alpha)\Gamma(\alpha)} \int_0^\tau (\tau-\vartheta)^{\alpha-1} \left(|\lambda_1| \epsilon_5 |\mathrm{u}(\bar{\boldsymbol{x}},\tau) - \overline{\mathrm{u}}(\bar{\boldsymbol{x}},\tau)| + |\lambda_2| |\mathrm{u}(\bar{\boldsymbol{x}},\tau) - \overline{\mathrm{u}}(\bar{\boldsymbol{x}},\tau)| + \epsilon_7 \right) d\vartheta
\end{aligned}$$

taking the supremum norm:

$$\begin{aligned}
\|\mathrm{u} - \overline{\mathrm{u}}\|_\infty &\leq \frac{(1-\alpha)}{\beta(\alpha)} \left(|\lambda_1| \epsilon_5 \|\mathrm{u} - \overline{\mathrm{u}}\|_\infty + |\lambda_2| \|\mathrm{u} - \overline{\mathrm{u}}\|_\infty \right) \\
&\quad + \frac{\alpha}{\beta(\alpha)\Gamma(\alpha)} \int_0^\tau (\tau-\vartheta)^{\alpha-1} \left(|\lambda_1| \epsilon_5 \|\mathrm{u} - \overline{\mathrm{u}}\|_\infty + |\lambda_2| \|\mathrm{u} - \overline{\mathrm{u}}\|_\infty + \epsilon_7 \right) d\vartheta \\
&\leq \left(\frac{(1-\alpha)}{\beta(\alpha)} + \frac{\tau^\alpha}{\beta(\alpha)\Gamma(\alpha)} \right) \left(|\lambda_1| \epsilon_5 \|\mathrm{u} - \overline{\mathrm{u}}\|_\infty + |\lambda_2| \|\mathrm{u} - \overline{\mathrm{u}}\|_\infty \right) \\
&\quad + \frac{\epsilon_7 \tau^\alpha}{\beta(\alpha)\Gamma(\alpha)} \Bigg) \\
&= \left(\frac{((1-\alpha)\Gamma(\alpha) + \tau^\alpha)(|\lambda_1|\epsilon_5 + |\lambda_2|)}{\beta(\alpha)\Gamma(\alpha)} \right) \|\mathrm{u} - \overline{\mathrm{u}}\|_\infty + \frac{\epsilon_7 \tau^\alpha}{\beta(\alpha)\Gamma(\alpha)}.
\end{aligned}$$

Rearranging, we get:

$$\left[1 - \left(\frac{((1-\alpha)\Gamma(\alpha) + \tau^\alpha)(|\lambda_1|\epsilon_5 + |\lambda_2|)}{\beta(\alpha)\Gamma(\alpha)} \right) \right] \|\mathrm{u} - \overline{\mathrm{u}}\|_\infty \leq \frac{\epsilon_7 \tau^\alpha}{\beta(\alpha)\Gamma(\alpha)}.$$

Since Eq.(6) ensures that $\frac{(1-\alpha)\Gamma(\alpha)+\tau^\alpha}{\Gamma(\alpha)\beta(\alpha)} \Big(\big(\epsilon_5|\lambda_1| + |\lambda_2|\big) \|\mathrm{u}_1 - \mathrm{u}_2\|_\infty \Big) < 1$, we have

$$\|\mathrm{u} - \overline{\mathrm{u}}\|_\infty \leq \mathcal{G}\epsilon.$$

where

$$\mathcal{G} = \frac{\tau^{\alpha}}{\left\{\beta(\alpha)\Gamma(\alpha) - [((1-\alpha)\Gamma(\alpha) + \tau^{\alpha})(|\lambda_1|\epsilon_5 + |\lambda_2|)]\right\}}.$$

Since $\mathcal{G} > 0$, the solution is Ulam-Hyers stable.

5. Proposed numerical method

The proposed numerical method for solving the TFDWE with the MABC derivative consists of three main steps: (a) discretization of the time variable via the Laplace transform, which converts the problem to the Laplace domain; (b) solution of the resulting boundary value problem in the Laplace domain using the CSCM; and (c) recovery of the time-domain solution by applying a numerical inverse Laplace transform based on a modified Talbot contour and the midpoint rule.

5.1. Laplace transform

The LT is applied to TFDWE (1)–(3) to discretize the time variable. Applying the LT to the model, we have:

$$\frac{\beta(\alpha)\left(s^{\alpha}\widehat{\mathrm{u}}(\bar{\boldsymbol{x}},s) - s^{\alpha-1}\mathrm{u}(\bar{\boldsymbol{x}},0) - s^{\alpha-2}\mathrm{u}_t(\bar{\boldsymbol{x}},0)\right)}{s^{\alpha}(1-\alpha)+\alpha} - \lambda_1\nabla^2\widehat{\mathrm{u}}(\bar{\boldsymbol{x}},s) - \lambda_2\widehat{\mathrm{u}}(\bar{\boldsymbol{x}},s) = \widehat{f}(\bar{\boldsymbol{x}},s),\ \bar{\boldsymbol{x}}\in\Theta$$

for $\bar{\boldsymbol{x}} \in \Theta$ with boundary condtions:

$$\mathrm{B}\widehat{\mathrm{u}}(\bar{\boldsymbol{x}},s) = \widehat{g_1}(\bar{\boldsymbol{x}},s), \quad \bar{\boldsymbol{x}}\in\partial\Theta,$$

the above expression can be written in operator form as:

$$\left\{\left(\frac{\beta(\alpha)s^{\alpha}}{s^{\alpha}(1-\alpha)+\alpha}\right)I - \lambda_1\pounds - \lambda_2 I\right\}\widehat{\mathrm{u}}(\bar{\boldsymbol{x}},s) = \widehat{H}(\bar{\boldsymbol{x}},s), \tag{9}$$

where:

$$\widehat{H}(\bar{\boldsymbol{x}},s) = \frac{\beta(\alpha)s^{\alpha-1}g_2(\bar{\boldsymbol{x}})}{s^{\alpha}(1-\alpha)+\alpha} + \frac{\beta(\alpha)s^{\alpha-2}g_3(\bar{\boldsymbol{x}})}{s^{\alpha}(1-\alpha)+\alpha} + \widehat{f}(\bar{\boldsymbol{x}},s)$$

and the boundary conditions remain

$$\mathrm{B}\widehat{\mathrm{u}}(\bar{\boldsymbol{x}},s) = \widehat{g_1}(\bar{\boldsymbol{x}},s),\ \bar{\boldsymbol{x}}\in\partial\Theta. \tag{10}$$

Here, $\mathcal{L} = \nabla^2$ denotes the Laplacian operator. The spatial operators in Eqs. (9)–(10) are then discretized using the CSCM, which transforms the problem into a system of linear equations in the Laplace domain. This system is solved for each value of the Laplace parameter s. Finally, the solution in the time domain, $u(\bar{\boldsymbol{x}},t)$, is recovered by applying a numerical inverse Laplace transform.

5.2. Spectral method

The CSCM is employed in this section to discretize the spatial operators in the transformed system given in Eqs. (9)–(10). This method uses Lagrange interpolation polynomials (LIPs) based on Chebyshev nodes to approximate the solution over the domain Θ, which is $[-1,1]$ in 1D, $[-1,1]^2$ in 2D, and $[-1,1]^3$ in 3D, with $\bar{\boldsymbol{x}} = x$, (x,y), or (x,y,z) respectively. For the 1D case the solution $\widehat{\mathrm{u}}(x,s)$ is approximated as [33, 34]:

$$\mathfrak{I}_{\mathrm{N}}(x) = \sum_{=0}^{\mathrm{N}} \ell(x)\widehat{\mathrm{u}}(x,s),$$

where $\ell(x)$ are LIPs defined as Chebyshev nodes x, which are given by:

$$x = \left\{ \cos\left(\frac{\pi}{\mathrm{N}}\right) \right\}_{=0}^{\mathrm{N}}. \tag{11}$$

and

$$\ell(x) = \prod_{j=0, j\neq}^{\mathrm{N}} \frac{x - x_j}{x - x_j}, \tag{12}$$

The derivative $\frac{\partial \widehat{\mathrm{u}}(x)}{\partial x}$ is approximated using the differentiation matrix $_{\mathrm{N}}$, with elements:

$$\{_{\mathrm{N}}\}_{k,} = \ell'(x_k),\ k,\ = 0,1,2,...,\mathrm{N},$$

where the off-diagonal entries are:

$$\{_{\mathrm{N}}\}_{k,} = \frac{\upsilon}{\upsilon_k(x_k - x)},\ k \neq ,$$

with $\upsilon^{-1} = \prod_{k=0,k\neq}^{\mathrm{N}}(x_k - x)$, and the diagonal entries:

$$\{_{\mathrm{N}}\}_{k,} = -\sum_{=0,\ \neq k}^{\mathrm{N}} \{_{\mathrm{N}}\}_{k,},\ k = 0,1,2,..,\mathrm{N}.$$

Higher derivatives are obtained as:

$$\{^{(\mathrm{m})}_{\mathrm{N}}\}_{k,} = \ell^{(\mathrm{m})}(x_k).$$

For 1D, $\pounds_{\boldsymbol{Disc}} = \frac{\partial^2}{\partial x^2}$, approximated by $^2_{\mathrm{N}}$. The authors of [35, 36] developed an effective and precise formulation for constructing differentiation matrices. Specifically, [35] provides a practical method for deriving the matrix $^{\mathrm{m}}_{\mathrm{N}}$, presented as follows:

$$\{^{(\mathrm{m})}_{\mathrm{N}}\}_k = \frac{\mathrm{m}}{x_k - x}\left(\frac{\upsilon}{\upsilon_k}\{^{(\mathrm{m}-1)}_{\mathrm{N}}\}_{kk} - \{^{(\mathrm{m}-1)}_{\mathrm{N}}\}_k\right),\ k \neq .$$

For $\Gamma = [-1,1]^2$, the points $\bar{\boldsymbol{x}}_k$ are presented as follows:

$$\bar{\boldsymbol{x}}_k = \left(\cos\left(\frac{\pi}{\mathrm{N}}\right), \cos\left(\frac{\pi k}{\mathrm{N}}\right)\right), \ , k = 0,1,2,...,\mathrm{N}.$$

The LIPs are:

$$\ell_k(\bar{\boldsymbol{x}}) = \ell(x)\ell_k(y), \ , k = 0,1,2,...,\mathrm{N}. \tag{13}$$

where $\ell_k(\bar{\boldsymbol{x}}_k) = \sigma_k$. The 2^{nd}-order derivatives of the LIPs (13) are given as:

$$\frac{\partial^2 \ell_k(\bar{\boldsymbol{x}}_{rp})}{\partial x^2} = \ell''(x_r)\ell_k(y_p) = \{{}^2_{\mathrm{N}}\}_r \sigma_{kp},$$

$$\frac{\partial^2 \ell_k(\bar{\boldsymbol{x}}_{rp})}{\partial y^2} = \ell(x_r)\ell''_k(y_p) = \sigma_r \{{}^2_{\mathrm{N}}\}_{pk},$$

where ${}^2_{\mathrm{N}}$ is the 2^{nd} order differentiation matrix. Employing $\pounds$ on $\ell_k(\bar{\boldsymbol{x}}_{rp})$ at $\bar{\boldsymbol{x}}_{rp}$ gives

$$\pounds(\ell_k(\bar{\boldsymbol{x}}_{rp})) = \left(\{{}^2_{\mathrm{N}}\}_r \sigma_{kp} + \sigma_r \{{}^2_{\mathrm{N}}\}_{pk} \right) \tag{14}$$

Thus, the discretized representation of the linear differential operator $\pounds$, derived using the CSCM, is given as:

$$\pounds_{\boldsymbol{Disc}} = I_{\mathrm{N}} \otimes {}^2_{\mathrm{N}} + {}^2_{\mathrm{N}} \otimes I_{\mathrm{N}}, \qquad (2D) \tag{15}$$

where $\otimes$ represent the Kronecker product. In 3D, the domain is $\Gamma = [-1,1]^3$, and the Chebyshev nodes are:

$$\bar{\boldsymbol{x}}_{\ell km} = \left(\cos\left(\frac{\pi \ell}{\mathrm{n}}\right), \cos\left(\frac{\pi k}{\mathrm{n}}\right), \cos\left(\frac{\pi m}{\mathrm{n}}\right)\right), \quad \ell, k, m = 0,1,\ldots,\mathrm{n}.$$

The associated LIPs in 3D are:

$$\ell_{km}(\bar{\boldsymbol{x}}) = \ell(x)\ell_k(y)\ell_m(z), \quad , k, m = 0,1,\ldots,\mathrm{n}, \tag{16}$$

where $\ell_{km}(\bar{\boldsymbol{x}}_{km}) = \sigma_{km}$, and the second-order derivatives are obtained as:

$$\frac{\partial^2 \ell_{km}(\bar{\boldsymbol{x}}_{rp\tau})}{\partial x^2} = \ell''(x_r)\ell_k(y_p)\ell_m(z_\tau) = \{{}^2_{\mathrm{n}}\}_r \sigma_{kp}\sigma_{mt},$$

$$\frac{\partial^2 \ell_{km}(\bar{\boldsymbol{x}}_{rp\tau})}{\partial y^2} = \ell(x_r)\ell''_k(y_p)\ell_m(z_\tau) = \sigma_r \{{}^2_{\mathrm{n}}\}_{pk}\sigma_{mt},$$

$$\frac{\partial^2 \ell_{km}(\bar{\boldsymbol{x}}_{rp\tau})}{\partial z^2} = \ell(x_r)\ell_k(y_p)\ell''_m(z_\tau) = \sigma_r\sigma_{kp}\{{}^2_{\mathrm{n}}\}_{tm},$$

where $\bar{\boldsymbol{x}}_{rp\tau} = (x_r, y_p, z_\tau)$. Applying $\pounds$ to $\ell_{km}(\bar{\boldsymbol{x}}_{rp\tau})$ at $\bar{\boldsymbol{x}}_{rp\tau}$ gives:

$$\pounds(\ell_{km}(\bar{\boldsymbol{x}}_{rp\tau})) = \left(\{{}^2_{\mathrm{n}}\}_r \sigma_{kp}\sigma_{m\tau} + \sigma_r \{{}^2_{\mathrm{n}}\}_{pk}\sigma_{m\tau} + \sigma_r\sigma_{kp}\{{}^2_{\mathrm{n}}\}_{\tau m}\right), \tag{17}$$

The discrete 3D Laplacian is

$$\pounds_{\boldsymbol{Disc}} = I_{\mathrm{N}} \otimes I_{\mathrm{N}} \otimes {}^{2}_{\mathrm{N}} + I_{\mathrm{N}} \otimes {}^{2}_{\mathrm{N}} \otimes I_{\mathrm{N}} + {}^{2}_{\mathrm{N}} \otimes I_{\mathrm{N}} \otimes I_{\mathrm{N}}, \quad (3D), \tag{18}$$

using matrix $\pounds_{\boldsymbol{Disc}}$ in Eq. (9), we obtain the discretized system as:

$$\left\{ \left(\frac{\beta(\alpha) s^{\alpha}}{s^{\alpha}(1-\alpha)+\alpha} \right) I - \lambda_1 \pounds_{\boldsymbol{Disc}} - \lambda_2 I \right\} \widehat{\mathrm{u}}(\bar{\boldsymbol{x}}, s) = \widehat{H}(\bar{\boldsymbol{x}}, s), \tag{19}$$

The conditions in Eq (10) are incorporating by considering the interpolation matrix $\pounds_{\boldsymbol{Disc}}$ and considering all points $\bar{\boldsymbol{x}}$. Furthermore, the rows of $\pounds_{\boldsymbol{Disc}}$ in correspondence with boundary nodes are replaced with unit vectors that have a one in accordance with the diagonal elements of $\pounds_{\boldsymbol{Disc}}$. Hence, the boundary conditions $\mathrm{B}\widehat{\mathrm{u}}(\bar{\boldsymbol{x}}, s) = \widehat{g_1}(\bar{\boldsymbol{x}}, s)$ in Eq (10) will be implemented directly [33]. Rearranging the columns and rows of the matrix $\pounds_{\boldsymbol{Disc}}$, the following block matrix is obtained.

$$\pounds_{\Gamma} = \begin{bmatrix} \mathcal{W} & \mathcal{F} \\ 0 & I \end{bmatrix},$$

where the non-zero block $\mathcal{W}$ and I is of size having order $(\mathrm{N}-\mathrm{N}_B)\times(\mathrm{N}-\mathrm{N}_B)$ and $\mathrm{N}_B \times \mathrm{N}_B$. Here N_B denotes the boundary nodes. Thus, the system (9)-(10) has the following form:

$$\pounds_{\Gamma} \widehat{\mathrm{u}}(\bar{\boldsymbol{x}}, s) = \begin{bmatrix} \widehat{H}(\bar{\boldsymbol{x}}, s) \\ \widehat{f}(\bar{\boldsymbol{x}}, s) \end{bmatrix}. \tag{20}$$

The solution $\widehat{u}(\bar{\boldsymbol{x}}, s)$ in the Laplace domain is determined by solving (20). The solution $u(\bar{\boldsymbol{x}}, t)$ of the original problem (1)–(3) is then recovered by applying the inverse Laplace transform to $\widehat{u}(\bar{\boldsymbol{x}}, s)$ as follows:

$$\mathrm{u}(\bar{\boldsymbol{x}}, \tau) = \frac{1}{2\pi i} \int_{\mu - i\infty}^{\mu + i\infty} e^{s\tau} \widehat{\mathrm{u}}(\bar{\boldsymbol{x}}, s) ds = \frac{1}{2\pi i} \int_{\Gamma_{\mathrm{c}}} e^{s\tau} \widehat{\mathrm{u}}(\bar{\boldsymbol{x}}, s) ds, \ Re(s) > 0, \tag{21}$$

5.3. Contour selection and quadrature

One of the most effective approaches for computing Eq. (21) is to deform the integration contour Γ_{c} into the left half plane to ensure the integrand decays, followed by applying the quadrature methods. This idea traces back to 1950, originating in the work of Talbot's doctoral student Green [37]. Talbot later published a paper [38] in which he generalized and improved the work of Green. Talbot suggested to deform the integration contour into a contour Γ_{c} that begins and ends in the left plane, such that $Re(s) \longrightarrow -\infty$ as $|s| \to \infty$. In literature, many popular contours have been proposed, such as Talbot's contour [29, 38], the parabolic and hyperbolic contours [39]. The work utilizes the modified Talbot's contour proposed in [29] as:

$$\Gamma_{\mathrm{c}} : s = s(\xi), \qquad \xi \in [-\pi, \ \pi], \ Re\big(s(\pm\pi)\big) = -\infty, \tag{22}$$

we have

$$s(\xi) = \frac{\mathrm{M_T}}{\tau}\varepsilon(\xi),\ \varepsilon(\xi) = -\theta_1 + \theta_2\xi\cot(\theta_3\xi) + \theta_4 i\xi, \tag{23}$$

where the user will select the parameters $\theta_1,\ \theta_2,\ \theta_3$, and θ_4. From (23) and (21), we have

$$\mathrm{u}(\bar{\boldsymbol{x}},\ \tau) = \frac{1}{2\pi i}\int_{-\pi}^{\pi} e^{s(\xi)\tau}\widehat{\mathrm{u}}(\bar{\boldsymbol{x}}, s(\xi))s'(\xi)d\xi. \tag{24}$$

Fast and accurate approximation of (24) can be achieved using trapezoidal or midpoint rule [29]. This work focuses on the midpoint rule with a step $\hbar = \frac{2\pi}{\mathrm{M_T}}$ given by:

$$\mathrm{u_{app}}(\bar{\boldsymbol{x}}, \tau) \approx \frac{1}{\mathrm{M_T} i}\sum_{k=1}^{\mathrm{M_T}} e^{s(\xi_k)\tau}\widehat{\mathrm{u}}(\bar{\boldsymbol{x}}, s(\xi_k))s'(\xi_k), \qquad \xi_k = -\pi + (\frac{2k-1}{2})\hbar. \tag{25}$$

5.3.1. Error analysis

The error analysis is performed in three stages:
Step 1: In the first step, the LT is employed, which transforms the given problem into a time-independent problem, since this transformation is exact, no error is introduced in this step.
Step 2: In step 2, we employ the CSCM discretization technique to solve the transformed problem, with the corresponding error estimate developed below:
Utilizing the points in Eq. (11) and the LPs in Eq. (12), the interpolation operator presented in [34] is expressed as:

$$\mathfrak{I}_{\mathrm{N}} : \mathrm{C}(\Theta) \to \mathfrak{P}_{\mathrm{N}}, \quad \mathfrak{I}_{\mathrm{N}}(\widehat{\mathrm{u}}) = \sum_{=0}^{\mathrm{N}} \widehat{\mathrm{u}}(x, s)\ell(x). \tag{26}$$

Following the technique in [40], we establish the error bound. Let $\mathrm{Q_N}$ be a constant; then, the stability estimate is expressed as:

$$\|\mathfrak{I}_{\mathrm{N}}(\widehat{\mathrm{u}})\|_\infty \le \mathrm{Q_N}\|\widehat{\mathrm{u}}\|_\infty, \quad \forall\ \widehat{\mathrm{u}} \in \mathrm{C}[-1, 1]. \tag{27}$$

Additionally,

$$\mathfrak{I}_{\mathrm{N}}(\widehat{\mathrm{u}}) = \widehat{\mathrm{u}}, \quad for \ \ all \ \ \widehat{\mathrm{u}} \in \mathfrak{P}_{\mathrm{N}}. \tag{28}$$

For Chebyshev interpolation, the stability constant grows logarithmically with N:

$$\mathrm{Q_N} = 1 + \left(\frac{ln(1+\mathrm{N})\pi}{2}\right) \le (\mathrm{N}+1). \tag{29}$$

For any $\widehat{\mathrm{u}} \in \mathcal{C}^{\mathrm{N}+1}[-1, 1]$, the interpolation error bound is expressed as [**?**]:

$$\|\widehat{\mathrm{u}} - \mathfrak{I}_{\mathrm{N}}(\widehat{\mathrm{u}})\|_\infty \le \frac{2^{-\mathrm{N}}}{\Gamma(\mathrm{N}+2)}\|\widehat{\mathrm{u}}^{\mathrm{N}+1}\|_\infty. \tag{30}$$

Theorem 1. [40] If $\widehat{\mathrm{u}} \in \mathrm{C}^{(\mathrm{N}+1)}[-1,1]$, then for $q = 0, 1, ..., \mathrm{N}$

$$\|\widehat{\mathrm{u}}^{(q)} - \mathfrak{I}_{\mathrm{N}}(\widehat{\mathrm{u}})^{(q)}\|_\infty \leq \frac{2(\mathrm{Q}_{\mathrm{N}}^{(q)}+1)}{\Gamma(\mathrm{N}-q+2)}\left(\frac{1}{2}\right)^{(\mathrm{N}-q+1)}\|\widehat{\mathrm{u}}^{(\mathrm{N}+1)}\|_\infty, \tag{31}$$

where

$$\mathrm{Q}_{\mathrm{N}}^{(q)} = \frac{\mathrm{Q}_{\mathrm{N}}}{\Gamma(q+1)}\left(\frac{\Gamma(\mathrm{N}+1)}{\Gamma(\mathrm{N}-q+1)}\right).$$

Application to 1D case:

For $1D$ operator $\pounds\widehat{\mathrm{u}} = \frac{\partial^2\widehat{\mathrm{u}}(\bar{\boldsymbol{x}},t)}{\partial x^2}$, the error bound is expressed as:

$$\begin{aligned}
\mathrm{E} &= \left\|\left\{\left(\frac{\beta(\alpha)s^\alpha}{s^\alpha(1-\alpha)+\alpha}\right)I - \lambda_1\pounds - \lambda_2 I\right\}\widehat{\mathrm{u}} - \left\{\left(\frac{\beta(\alpha)s^\alpha}{s^\alpha(1-\alpha)+\alpha}\right)I - \lambda_1\pounds - \lambda_2 I\right\}\mathfrak{I}_{\mathrm{N}}\widehat{\mathrm{u}}\right\|_\infty \\
&= \left\|\left(\frac{\beta(\alpha)s^\alpha}{s^\alpha(1-\alpha)+\alpha}\right)(\widehat{\mathrm{u}} - \mathfrak{I}_{\mathrm{N}}\widehat{\mathrm{u}}) - \lambda_1\pounds(\widehat{\mathrm{u}} - \mathfrak{I}_{\mathrm{N}}\widehat{\mathrm{u}}) - \lambda_2(\widehat{\mathrm{u}} - \mathfrak{I}_{\mathrm{N}}\widehat{\mathrm{u}})\right\|_\infty \\
&\leq \left|\left(\frac{\beta(\alpha)s^\alpha}{s^\alpha(1-\alpha)+\alpha}\right)\right|\|\widehat{\mathrm{u}} - \mathfrak{I}_{\mathrm{N}}\widehat{\mathrm{u}}\|_\infty + |\lambda_1|\|\pounds(\widehat{\mathrm{u}} - \mathfrak{I}_{\mathrm{N}}\widehat{\mathrm{u}})\|_\infty + |\lambda_2|\|\widehat{\mathrm{u}} - \mathfrak{I}_{\mathrm{N}}\widehat{\mathrm{u}}\|_\infty,
\end{aligned}$$

since s^α, and $\beta(\alpha)$ are constants, so we have

$$\mathrm{E} \leq \left(\left(\frac{\beta(\alpha)s^\alpha}{s^\alpha(1-\alpha)+\alpha}\right) + \lambda_2\right)\frac{2^{-\mathrm{N}}}{\Gamma(\mathrm{N}+2)}\|\widehat{\mathrm{u}}^{\mathrm{N}+1}\|_\infty + |\lambda_1|\frac{2(\mathrm{Q}_{\mathrm{N}}^{(2)}+1)}{\Gamma(\mathrm{N})}\left(\frac{1}{2}\right)^{(\mathrm{N}-1)}\|\widehat{\mathrm{u}}^{(\mathrm{N}+1)}\|_\infty.$$

Hence, we obtain

$$\mathrm{E} \leq \mathcal{K}\|\widehat{\mathrm{u}}^{(\mathrm{N}+1)}\|_\infty,$$

where $\mathcal{K}$ is a constant combining all coefficients of $\|\widehat{\mathrm{u}}^{(\mathrm{N}+1)}\|_\infty$. For higher dimensions see [40].

Step 3: The final step is the numerical approximation of the integral in Eq.(24) via Talbot's method, implemented with the midpoint rule, whose convergence rate depends on the following factors:

- The contour selection,
- The step size.

Parameters for optimal accuracy as determined in [29] are:

$$\theta_1 = 0.61220,\ \theta_2 = 0.50170,\ \theta_3 = 0.640700, \text{and } \theta_4 = 0.26450s,$$

and corresponding error estimate:

$$E^{est} = |\mathrm{u}_{app}(\bar{\boldsymbol{x}},\tau) - \mathrm{u}(\bar{\boldsymbol{x}},\tau)| = \mathrm{O}(exp((-1.35800)\mathrm{M}_\mathrm{T})).$$

6. Numerical Experiments

The performance of the proposed method is evaluated using three numerical examples. Accuracy is measured with two error metrics: the absolute error (L_{Abs}) and the maximum absolute error (L_∞), defined as:

$$L_{Abs} = \left| \mathrm{u}(\bar{\boldsymbol{x}}_k,\ \tau) - \mathrm{u}_{app}(\bar{\boldsymbol{x}}_k, \tau) \right|,$$

$$L_\infty = \max_{1 \le k \le \mathrm{N}} \left| \mathrm{u}(\bar{\boldsymbol{x}}_k, \tau) - \mathrm{u}_{app}(\bar{\boldsymbol{x}}_k, \tau) \right|,$$

where $\mathrm{u}(\bar{\boldsymbol{x}}, \tau)$ and $\mathrm{u}_{app}(\bar{\boldsymbol{x}}, \tau)$ denote the exact and approximate solutions, respectively. Here, N and M_Q denote the number of Chebyshev nodes and quadrature nodes, respectively. All simulations employ fixed parameters $\lambda_1 = 1$ and $\lambda_2 = 0$. For each example, the source term, initial conditions, and boundary conditions are derived from the exact solution.

Example 1

In the first example, we consider the 1D version of (1)–(3) with $\lambda_1 = 1$, $\lambda_2 = 0$, and exact solution $\mathrm{u}(x, \tau) = \sin(\pi x)\tau^2$. The performance of the proposed numerical method is evaluated through comprehensive error analysis and computational benchmarks. Table 1 shows the L_∞ error norms for varying Chebyshev nodes N and quadrature points (M_Q), demonstrating both computational efficiency and high accuracy. The solution accuracy is verified in Figure 1a, where the upper panel shows excellent agreement between exact and approximate solutions, while the lower panel depicts the corresponding pointwise absolute error distribution, confirming the method's high accuracy. Further, Figure 1b further examines solution accuracy for different values of α, showing consistent and stable numerical behavior.

Two major features are shown by convergence analysis: Up to $M_Q = 36$, Figure 2a demonstrates ideal quadrature convergence, after that, there is a slight increase in the error, most likely as a result of numerical conditioning effects. Similarly, spectral convergence with respect to spatial discretization is shown in Figure 2b, with slight error variation at higher N values caused by the round-off errors in the Chebyshev differentiation matrices.

Figures 3a and 3b quantify parametric sensitivity by plotting the L_∞ error dependence on t and α, respectively, both showing accurate results. The surface and contour plots (Figures 4a and 4b) in the $\alpha - \tau$ plane show the whole error nature and provide a thorough proof of the method's stability over the whole domain. Overall, these findings demonstrate that the proposed scheme achieves the following: (i) uniform stability for various values of α; (ii) exponential convergence in quadrature approximation; and (iii) spectral accuracy in spatial discretization. Thus, the method represents an effective technique for Solving fractional-order PDE problems.

Table 1: Errors norms for Example 1 with varying M_Q, α, and N.

M_Q	N	$\alpha = 1.5$		$\alpha = 1.75$	
		L_∞	C.Time(s)	L_∞	C.Time(s)
36	400	1.1419×10^{-12}	0.270315	2.2197×10^{-12}	0.434348
	500	6.2560×10^{-12}	1.212901	5.1609×10^{-12}	1.193002
	600	1.1793×10^{-12}	1.119774	2.7161×10^{-12}	0.904267
	700	7.3037×10^{-12}	1.541679	3.0467×10^{-12}	1.403863
26	850	1.6612×10^{-11}	1.114587	1.1432×10^{-11}	1.473688
28		3.2163×10^{-12}	1.106680	1.2373×10^{-11}	1.363364
30		4.2749×10^{-12}	1.425263	1.2061×10^{-11}	1.471200
32		7.5047×10^{-12}	2.004526	6.4597×10^{-12}	1.563570
34		5.1494×10^{-12}	1.505562	6.6363×10^{-12}	1.666364

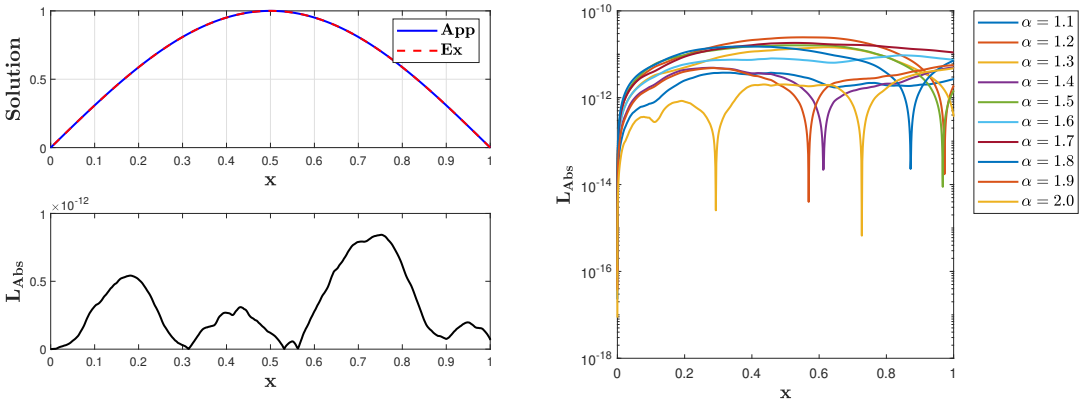

(a) (b)

Figure 1: (a) Comparison of approximate and exact solutions in the subplot 1 and the L_{Abs} in the subplot 2 N = 700, $M_Q = 36$ (Example 1). (b) Comparison of L_{Abs} for different α with N = 1000, $M_Q = 34$ (Example 1).

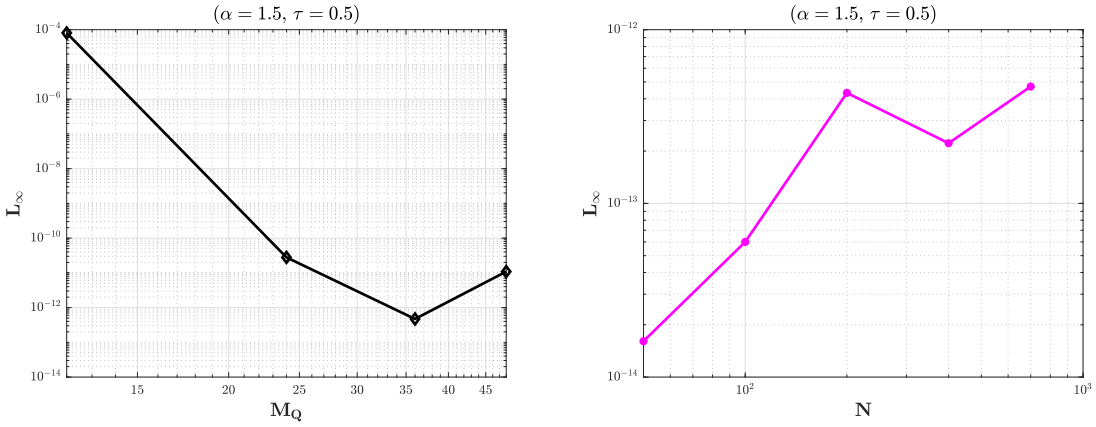

(a) (b)

Figure 2: (a) Graph of L_∞ vs quadrature nodes M_Q with N = 700 (Example 1). (b) Graph of L_∞ vs quadrature nodes N with $M_Q = 36$ (Example 1).

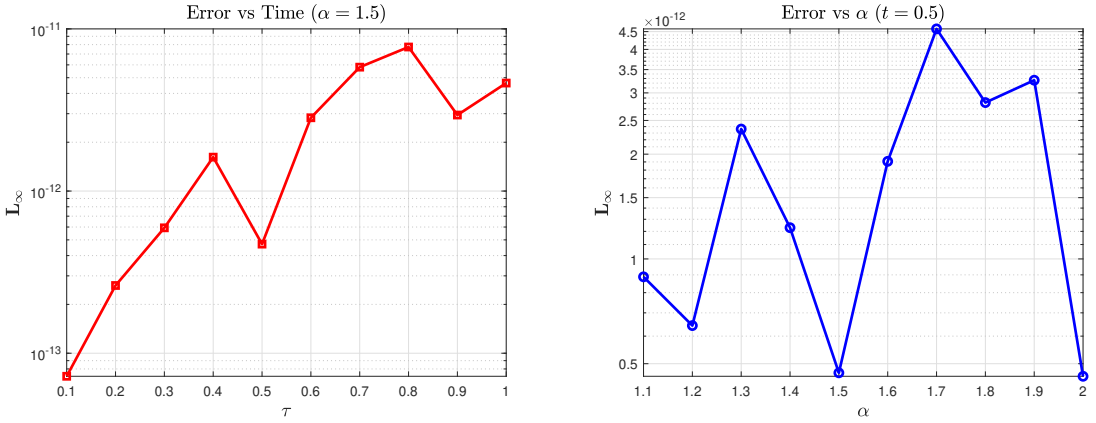

(a) (b)

Figure 3: (a) Graph of L_∞ vs τ with $M_Q = 36$ and N = 700 (Example 1). (b) Graph of L_∞ vs fractional order α with N = 700 and $M_Q = 36$ (Example 1).

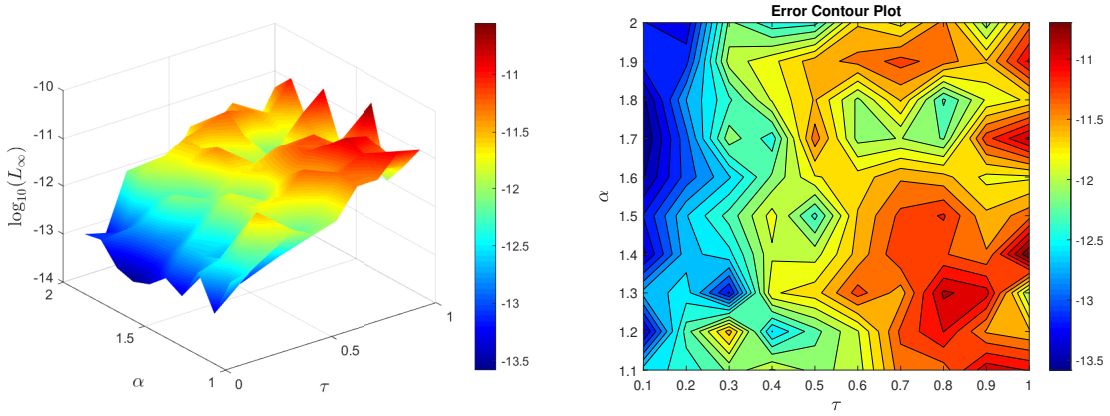

(a) (b)

Figure 4: (a) The graph shows L_∞ error in $\tau\alpha$ plane with $M_Q = 36$ and N = 700 (Example 1). (b) Contour plot of L_∞ in $\tau\alpha$ plane with $M_Q = 36$ and N = 700 (Example 1).

Example 2

In the second example, we consider the 2D version of (1)–(3) with $\lambda_1 = 1$, $\lambda_2 = 0$, and exact solution $u(x, \tau) = (1 - x^2 - y^2)\tau.^3$. The performance of the proposed numerical method is validated through detailed error analysis and computational tests. The L_∞ error for various values of N and quadrature points M_Q is shown in Table 2, showing both high accuracy and computational efficiency. The numerical solution of example 2 is shown in Figure 5a, and the surface plot presented in Figure 5b shows the absolute error distribution demonstrating stable numerical performance.

Figure 6a demonstrates perfect quadrature convergence up to $M_Q = 36$, after which the error experiences a small rise. Spectral convergence with respect to spatial discretization is evident in Figure 6b, where minor error oscillations appear at higher orders because of round-off errors in Chebyshev differentiation matrices. Figure 7a shows the dependence of L_∞ on τ for $1.1 \leq \alpha \leq 1.9$, while Figure 7b shows its dependence on α for $\tau = \{0.1, 0.4, 0.7, 1\}$, both demonstrating consistently high accuracy. Figures 8a and 8b present comprehensive error visualization using surface and contour plots in the $\alpha\tau$ plane, demonstrating the method's robust stability across the entire parameter domain.

Table 2: Errors norms for Example 2 with varying M_Q, α, and N.

M_Q	N	$\alpha = 1.5$		$\alpha = 1.75$	
		L_∞	C.Time(s)	L_∞	C.Time(s)
24	441	3.3135×10^{-9}	0.525874	3.3135×10^{-9}	0.430171
	784	3.3137×10^{-9}	1.371348	3.3135×10^{-9}	1.370788
	900	3.3135×10^{-9}	1.790163	3.3138×10^{-9}	2.238885
	1089	3.3135×10^{-9}	3.175910	3.3135×10^{-9}	3.317322
26	1681	5.4329×10^{-10}	9.138562	4.3794×10^{-10}	9.125002
28		7.1942×10^{-10}	9.830315	2.2237×10^{-10}	9.696946
30		3.7555×10^{-10}	10.442032	4.5945×10^{-10}	10.396021
32		7.4227×10^{-10}	11.273246	7.7937×10^{-10}	11.177015
34		3.1544×10^{-10}	13.683367	5.2071×10^{-10}	12.233212

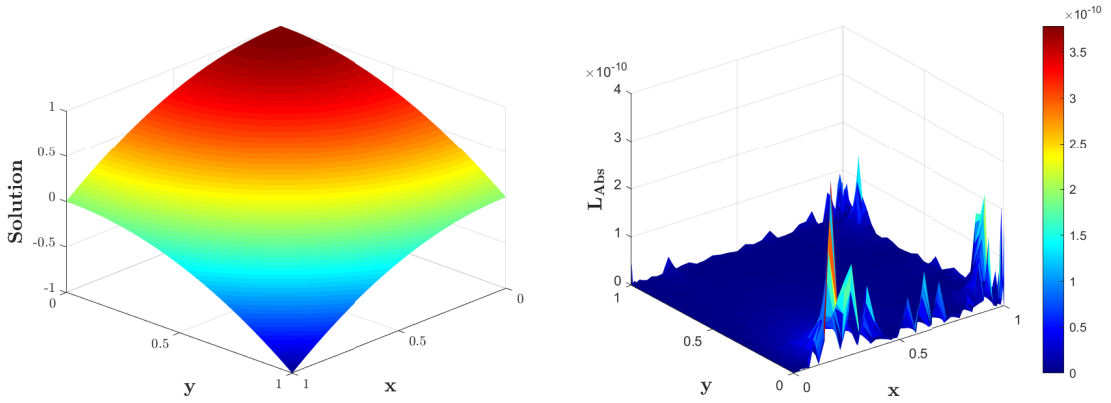

(a) (b)

Figure 5: (a) Comparison of approximate and exact solutions in the subplot 1 and the L_{Abs} in the subplot 2 N = 1681, $M_Q = 36$ (Example 2). (b) Plot of L_{Abs} of the method N = 1681, $M_Q = 36$ (Example 2).

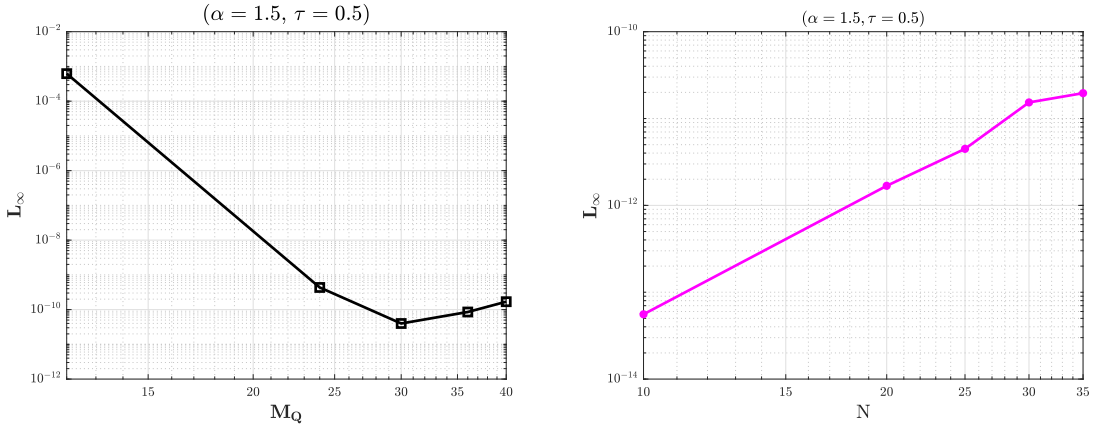

(a) (b)

Figure 6: (a) Graph of L_∞ vs quadrature nodes M_Q with N = 1681 (Example 2). (b) Graph of L_∞ vs quadrature nodes N with $M_Q = 36$ (Example 2).

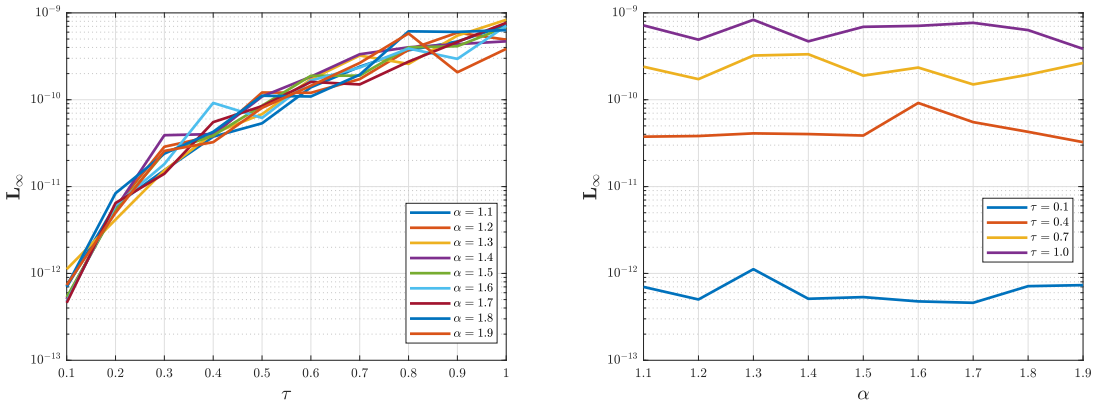

(a) (b)

Figure 7: (a) Graph of L_∞ vs τ with $M_Q = 36$ and N = 1681 (Example 2). (b) Graph of L_∞ vs fractional order α with N = 1681 and $M_Q = 36$ (Example 2).

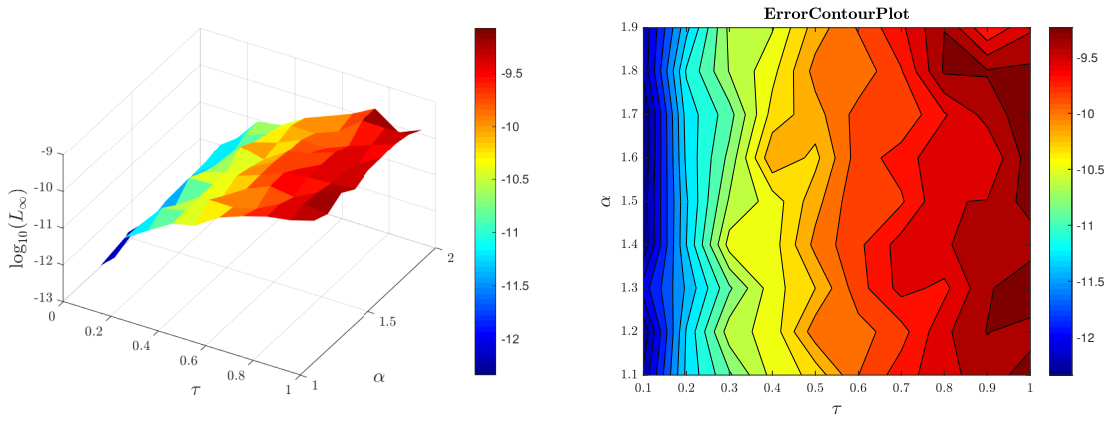

(a) (b)

Figure 8: (a) The graph shows the L_∞ error in $\tau\alpha$ plane with $M_Q = 36$ and N = 1681 (Example 2). (b) Contour plot of L_∞ in $\tau\alpha$ plane with $M_Q = 36$ and N = 1681 (Example 2).

Example 3

In the third example, we consider the 3D version of (1)–(3) with $\lambda_1 = 1$, $\lambda_2 = 0$, and exact solution $u(x, \tau) = \exp(x + y + z)\tau^3$. The L_∞ error for various values of N and quadrature points M_Q is shown in Table 3, showing both high accuracy and computational efficiency. The slice plots of numerical solution and absolute error computed usingN = 1331, $M_Q = 36$, $\tau = 1$, and $\alpha = 1.5$ are presented in Figures 9a and 9b respectively. A highly efficient performance is evident. The variation of L_∞ vs M_Q is presented in Figure 10a computed with N = 1728, $\alpha = 1.5$, and $\tau = 1$. Similarly, the variation of L_∞ vs N is shown in Figure 10b computed with $M_Q = 30$, $\alpha = 1.5$, and $\tau = 1$. Figures 11a and 11b presents the dependence of L_∞ on τ and α respectively, both demonstrate high accuracy. Further, Figures 12a show the error distribution in the αt plane. The contour slice plot of absolute error is presented in Figure 12b. Overall, it is evident that the method has the capability of solving fractional-order three-dimensional problems with high accuracy without facing any time instability issues.

Table 3: Errors norms for Example 2 with varying M_Q, α, and N.

M_Q	N	$\alpha = 1.5$		$\alpha = 1.75$	
		L_∞	C.Time(s)	L_∞	C.Time(s)
24	729	2.2140×10^{-9}	1.265030	2.2140×10^{-9}	1.013569
	1331	2.2140×10^{-9}	5.213977	2.2140×10^{-9}	4.466417
	2197	2.2140×10^{-9}	17.880434	2.2140×10^{-9}	15.620776
	3375	2.2140×10^{-9}	58.898524	2.2140×10^{-9}	52.157271
26	1331	1.7283×10^{-10}	5.531386	1.7283×10^{-10}	4.843518
28		3.9919×10^{-11}	6.134771	3.1216×10^{-11}	5.339569
30		2.4134×10^{-11}	6.425285	1.8025×10^{-11}	5.591827
32		2.6654×10^{-11}	5.969752	4.6171×10^{-11}	6.005012
34		3.5469×10^{-11}	6.343325	3.9908×10^{-11}	6.308768

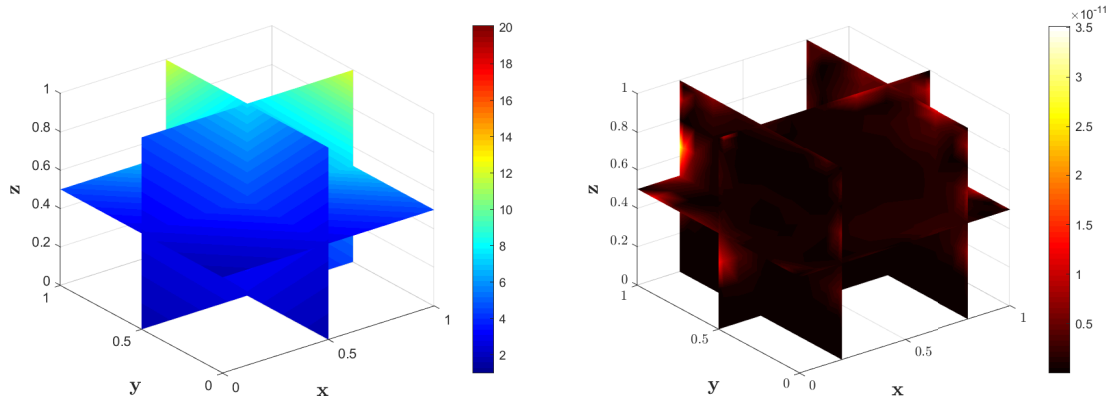

(a) (b)

Figure 9: (a) The slice plot of numerical solution with N = 1331, $M_Q = 36$, $\tau = 1$, and $\alpha = 1.5$ (Example 3). (b) The slice plot of L_{Abs} with N = 1331, $M_Q = 36$, $\tau = 1$, and $\alpha = 1.5$ (Example 3).

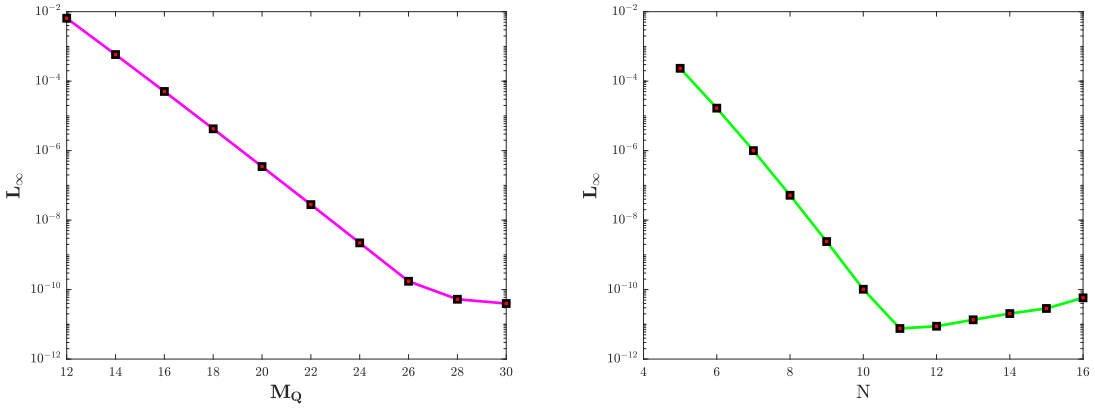

(a) (b)

Figure 10: (a) Graph of L_∞ vs quadrature nodes M_Q with N = 1728 (Example 3). (b) Graph of L_∞ vs quadrature nodes N with $M_Q = 30$ (Example 3).

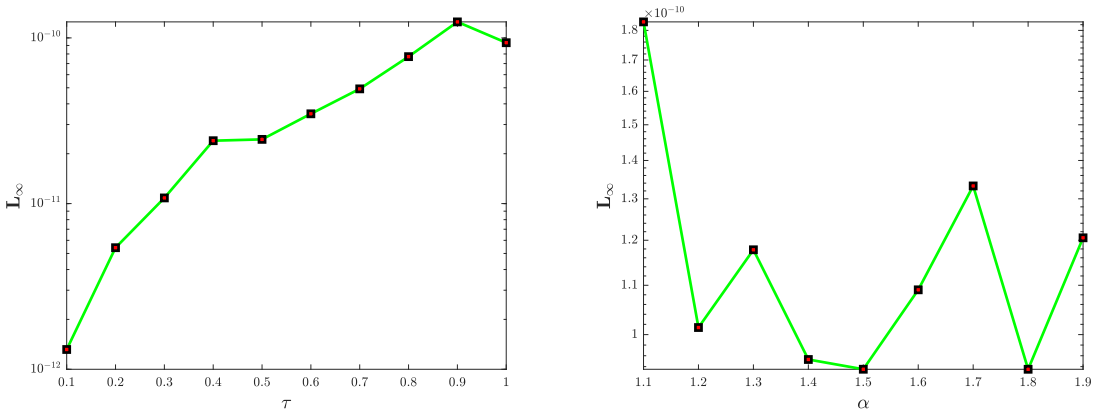

(a) (b)

Figure 11: (a) Graph of L_∞ vs τ with $M_Q = 36$ and N = 1728 (Example 3). (b) Graph of L_∞ vs fractional order α with N = 1728 and $M_Q = 36$ (Example 3).

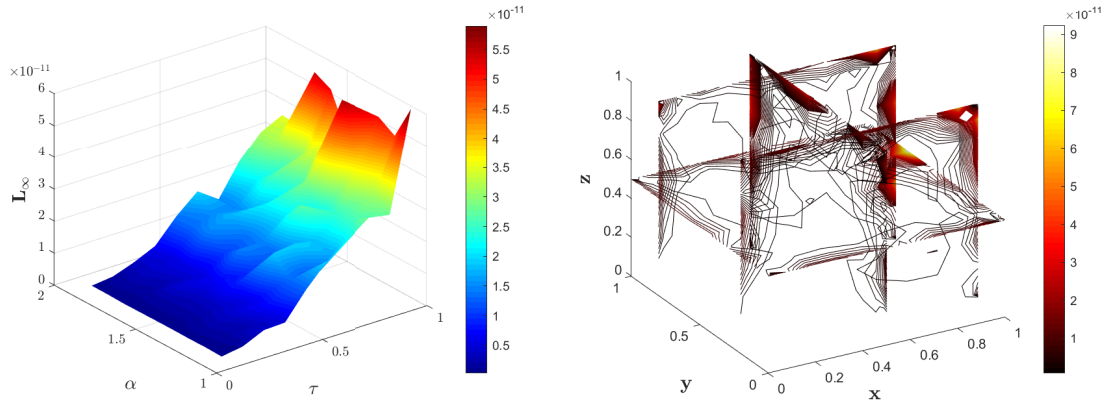

(a) (b)

Figure 12: (a) The graph shows the L_∞ error in $\tau\alpha$ plane with $M_Q = 30$ and N = 1728 (Example 3). (b) Contour plot of L_∞ in $\tau\alpha$ plane with $M_Q = 30$ and N = 1728 (Example 3).

7. Conclusion

The paper develops the LT based CSCM method for numerical modelling of time-fractional wave-diffusion equations including the MABC derivative. Unlike standard finite difference methods, the proposed numerical method implements the LT and the numerical inverse LT to efficiently handle the time-fractional derivative. It first utilizes the LT to transform the considered problem into a time-independent inhomogeneous problem in Laplace space. Then it employs the CSCM to discretize the spatial derivatives of the transformed problem. Finally, it uses the improved Talbot method to recover the time-domain solution.

Compared to conventional finite difference methods, the proposed LT-CSCM method provides two key features: (i) elimination of computationally expensive convolution integrals of fractional derivatives through LT; and (ii) unconditional stability independent of time-stepping constraints. The features enable efficient and accurate long-time simulation of diffusion-wave systems. The CSCM further improves the method's efficiency for high-dimensional problems, requiring fewer nodes while maintaining exponential convergence. Numerical experiments confirm the LT based CSCM's ability to handle multi-dimensional diffusion-wave problems.

Looking forward, the robustness and efficiency of the LT based CSCM scheme make it a strong candidate for simulating more complex fractional dynamical systems in applied mathematics and engineering. Future work will focus on adapting this methodology to solve fractional delay partial differential equations and coupled systems.

Acknowledgements

The authors A. Aloqaily and N. Mlaiki would like to thank Prince Sultan University for paying the publication fees for this work through TAS LAB.

Competing interests

There are no conflicting interests, according to the authors.

Author's contributions

Each author contributed equally to the writing of this work, and they have all read and approved the finished work.

Declarations

Ethical Approval Not applicable.
Funding This work did not receive any external funding.

References

[1] F. Mainardi. Fractional calculus: Theory and applications. *Mathematics*, 6(9):145, 2018.

[2] I. Podlubny. *Fractional differential equations: an introduction to fractional derivatives, fractional differential equations, to methods of their solution and some of their applications*, volume 198. Elsevier, 1998.

[3] Emad A Az-Zo'bi, Qais MM Alomari, Kallekh Afef, and Mustafa Inc. Dynamics of generalized time-fractional viscous-capillarity compressible fluid model. *Optical and Quantum Electronics*, 56(4):629, 2024.

[4] Mohammad A Al Zubi, Kallekh Afef, and Emad A Az-Zo'bi. Assorted spatial optical dynamics of a generalized fractional quadruple nematic liquid crystal system in nonlocal media. *Symmetry*, 16(6):778, 2024.

[5] S. G. Samko, A. A. Kilbas, and O. I. Marichev. *Fractional integrals and derivatives: Theory and applications*. Gordon and Breach Science Publishers, 1993.

[6] F. Mainardi. *Fractional calculus and waves in linear viscoelasticity*. World Scientific, 2010.

[7] M. Al-Refai and D. Baleanu. On an extension of the operator with mittag-leffler kernel. *Fractals*, 30(05):2240129, 2022.

[8] N. Shimizu and W. Zhang. Fractional calculus approach to dynamic problems of viscoelastic materials. *JSME International Journal Series C Mechanical Systems, Machine Elements and Manufacturing*, 42(4):825–837, 1999.

[9] K. Shah, H. Khalil, and R. A. Khan. Analytical solutions of fractional order diffusion equations by natural transform method. *Iranian Journal of Science and Technology, Transactions A: Science*, 42(3):1479–1490, 2018.

[10] M. Caputo. Linear models of dissipation whose q is almost frequency independent. *Annals of Geophysics*, 19(4):383–393, 1966.

[11] M. A. Khan and A. Atangana. Modeling the dynamics of hepatitis e via the mab derivative. *Journal of Applied Mathematics and Computing*, 55(1-2):345–358, 2017.

[12] F. Haq, K. Shah, G. ur Rahman, and M. Shahzad. Numerical solution of fractional order smoking model via laplace adomian decomposition method. *Alexandria Engineering Journal*, 57(2):1061–1069, 2018.

[13] K. Shah, M. A. Alqudah, F. Jarad, and T. Abdeljawad. Semi-analytical study of pine wilt disease model with convex rate under caputo-febrizio fractional order derivative. *Chaos, Solitons & Fractals*, 135:109754, 2020.

[14] F. Mainardi. The fundamental solutions for the fractional diffusion-wave equation. *Applied Mathematics Letters*, 9(6):23–28, 1996.

[15] O. P. Agrawal. Solution for a fractional diffusion-wave equation defined in a bounded domain. *Nonlinear Dynamics*, 29:145–155, 2002.

[16] J. Ren and Z. Z. Sun. Efficient numerical solution of the multi-term time fractional diffusion wave equation. *East Asian Journal on Applied Mathematics*, 5(1):1–28, 2015.

[17] F. Liu, M. Meerschaert, R. McGough, P. Zhuang, and Q. Liu. Numerical methods for solving the multi-term time-fractional wave-diffusion equation. *Fractional Calculus and Applied Analysis*, 16(1):9–25, 2013.

[18] Y. N. Zhang, Z. Z. Sun, and X. Zhao. Compact alternating direction implicit scheme for the two-dimensional fractional diffusion-wave equation. *SIAM Journal on Numerical Analysis*, 50(3):1535–1555, 2012.

[19] R. Salehi. A meshless point collocation method for 2-d multi-term time fractional diffusion-wave equation. *Numerical Algorithms*, 74:1145–1168, 2017.

[20] A. H. Bhrawy, E. H. Doha, D. Baleanu, and S. S. Ezz-Eldien. A spectral tau algorithm based on jacobi operational matrix for numerical solution of time fractional diffusion-wave equations. *Journal of Computational Physics*, 293:142–156, 2015.

[21] Y. Yang, Y. Chen, Y. Huang, and H. Wei. Spectral collocation method for the time-fractional diffusion-wave equation and convergence analysis. *Computers & Mathematics with Applications*, 73(6):1218–1232, 2017.

[22] M. H. Heydari, M. R. Hooshmandasl, F. M. Ghaini, and C. Cattani. Wavelets method for the time fractional diffusion-wave equation. *Physics Letters A*, 379(3):71–76, 2015.

[23] F. A. Shah, Kamran, Z. A. Khan, F. Azmi, and N. Mlaiki. A hybrid collocation method for the approximation of 2d time fractional diffusion-wave equation. *AIMS Mathematics*, 9(10):27122–27149, 2024.

[24] M. Dehghan, M. Safarpoor, and M. Abbaszadeh. Two high-order numerical algorithms for solving the multi-term time fractional diffusion-wave equations. *Journal of Computational and Applied Mathematics*, 290:174–195, 2015.

[25] J. Y. Yang, J. F. Huang, D. M. Liang, and Y. F. Tang. Numerical solution of fractional diffusion-wave equation based on fractional multistep method. *Applied Mathematical*

Modelling, 38(14):3652–3661, 2014.

[26] B. L. Buzbee, G. H. Golub, and C. W. Nielson. On direct methods for solving poisson's equations. *SIAM Journal on Numerical Analysis*, 7(4):627–656, 1970.

[27] J. P. Boyd. *Chebyshev and Fourier spectral methods*. Dover Publications, 2001.

[28] C. Canuto, M. Y. Hussaini, A. Quarteroni, and T. A. Zang. *Spectral methods: Fundamentals in single domains*. Springer Science & Business Media, 2006.

[29] B. Dingfelder and J. A. C. Weideman. An improved talbot method for numerical laplace transform inversion. *Numerical Algorithms*, 68(1):167–183, 2015.

[30] W. H. Huang, M. Samraiz, A. Mehmood, D. Baleanu, G. Rahman, and S. Naheed. Modified atangana-baleanu fractional operators involving generalized mittag-leffler function. *Alexandria Engineering Journal*, 75:639–648, 2023.

[31] R. Chawla, K. Deswal, D. Kumar, and D. Baleanu. A novel finite difference based numerical approach for modified atangana-baleanu caputo derivative. *AIMS Mathematics*, 7(9):17252–17268, 2022.

[32] P. Verma and M. Kumar. New existence, uniqueness results for multi-dimensional multi-term caputo time-fractional mixed sub-diffusion and diffusion-wave equation on convex domains. *Journal of Applied Analysis and Computation*, 11:1455–1480, 2021.

[33] L. N. Trefethen. *Spectral methods in MATLAB*. SIAM, Philadelphia, 2000.

[34] A. Shokri and S. Mirzaei. A pseudo-spectral based method for time-fractional advection-diffusion equation. *Computational Methods in Differential Equations*, 8(3):454–467, 2020.

[35] B. D. Welfert. Generation of pseudospectral differentiation matrices I. *SIAM Journal on Numerical Analysis*, 34(4):1640–1657, 1997.

[36] R. Baltensperger and M. R. Trummer. Spectral differencing with a twist. *SIAM Journal on Scientific Computing*, 24(5):1465–1487, 2003.

[37] J. S. Green. *The calculation of the time-responses of linear systems*. PhD thesis, Department of Applied Mathematics, Imperial College, London, 1955.

[38] A. Talbot. The accurate numerical inversion of laplace transforms. *IMA Journal of Applied Mathematics*, 23(1):97–120, 1979.

[39] J. Weideman and L. N. Trefethen. Parabolic and hyperbolic contours for computing the bromwich integral. *Mathematics of Computation*, 76(259):1341–1356, 2007.

[40] Steffen Börm, Lars Grasedyck, and Wolfgang Hackbusch. Introduction to hierarchical matrices with applications. *Engineering analysis with boundary elements*, 27(5):405–422, 2003.